CELL SEPARATION IN MICROFLUIDIC DEVICES

A Thesis Submitted to
the Graduate School of
İzmir Institute of Technology
in Partial Fulfillment of the Requirements for the Degree of

MASTER OF SCIENCE

in Bioengineering

by
Cemre ÖKSÜZ

July 2022
İZMİR

ACKNOWLEDGMENTS

First, I would like to express my thanks to my supervisor Assoc. Prof. Dr. H. Cumhur Tekin for supporting me, trusting my opinions, guiding and encouraging me during my MSc. thesis.

I would like thank to The Scientific and Technological Research Council of Turkey (217S518 and 119M052) for their financial support during my master studies. I wish to acknowledge the CBMS at the MicroTAS 2021 International Conference for considering me worth for LMIC Young Researcher Award.

I would like to thank Assoc. Prof. Dr. Özden Yalçın and to PhD student Elif Günyüz for giving the MCF-7 cells for the negative magnetophoresis microfluidic chip studies. I would express my thankfulness to Assoc. Prof. Dr. Can Biçmen from Dr. Suat Seren Chest Diseases and Chest Surgery Training and Research Hospital for the blood samples.

I would like to thank all Laboratory of Biomedical Micro and Nanosystems (LBMS) members for their support. I would like thank to Kerem Delikoyun for his support on Python coding. I thank my colleague Özge Özçelik for working on Maglev filtration together and Sadık Koç for his supports on whole blood separation experiments. In particular, I would like to thank Betül Karakuzu for her pure friendship, motivation and endless support from the beginning.

I would like to thank my soulmate Soner Sezer for his endless support for making dreams come true with me, love, and patient during my thesis. I express my gratitudes to my family Hatice Şahin, Nazan Şahin, especially, my sister Merve Kırmızı and my mother Emel Şahin for always trusting me throughout my life, holding my hand under all circumstances and never letting go and never letting me fall.

ABSTRACT

CELL SEPARATION IN MICROFLUIDIC DEVICES

Cell separation is used to separate homogeneous and individual cell classes from a heterogeneous cell population. The efficiency and purity of these separated cells are of great importance in personalized medicine, regenerative medicine, disease monitoring and drug testing as well as in the therapeutic and diagnostic research. In this thesis, different microfluidic approaches were presented for cell separation. With this regard, a closed channel vacuum-integrated microfluidic chip was developed using an air permeability of a Polydimethylsiloxane and density-based separation of microparticles was performed. Besides, a centrifugal microfluidic system, Spinochip, was developed with one reservoir as inlet and outlet for the first time and different fluid manipulations were shown in the system. The system was applied to clinical tests of hematocrit measurements and white blood cell estimation using real patient samples. The developed system offered correlated results with clinical results. In addition to closed channel microfluidics, negative-magnetophoresis microfluidic chip was demonstrated for the size-based separation of microparticles and cells. In this regard, capturing rate of breast cancer cells (MCF-7) and human monocyte cells (U937) was investigated. The results showed that the approaches presented here could promote to the microfluidic studies for size-based cell separation.

ÖZET

MİKROAKIŞKAN CİHAZLARDA HÜCRE AYRIŞTIRMA

Hücre ayrıştırma, homojen ve bireysel hücre sınıflarını heterojen bir hücre popülasyonundan homojen bir şekilde ayırmak için kullanılır. Bu ayrıştırılmış hücrelerin verimliliği ve saflığı, kişiselleştirilmiş tıp, rejeneratif tıp, hastalık izleme ve ilaç testlerinin yanı sıra terapötik ve teşhis araştırmalarında büyük önem taşımaktadır. Bu tezde, hücre ayrıştırması için farklı mikroakışkan yaklaşımlar sunulmuştur. Bu amaç ile, bir Polidimetilsiloksan çipin hava geçirgenliği kullanılarak kapalı kanallı, vakumla bütünleşik bir mikroakışkan çip geliştirilmiş ve mikroparçacıkların yoğunluğa dayalı olarak ayrışması başarılmıştır. Ayrıca, ilk kez giriş ve çıkış olarak tek hazneyi kullanan bir santrifüjlenebilir mikroakışkan sistem olan Spinochip geliştirilmiş ve sistemde farklı akışkan manipülasyonları gösterilmiştir. Sistem, gerçek hasta örnekleri kullanılarak hematokrit ölçümü ve beyaz kan hücresi sayımı gibi klinik testlere uygulamıştır. Geliştirilen sistem klinikle ilişkili sonuçlar vermiştir. Kapalı kanal mikroakışkanlara ek olarak, mikroparçacıkların ve hücrelerin boyuta dayalı olarak ayrılması için negatif-manyetoforez mikroakışkan çipi sunulmuştur. Bu bağlamda, insan monosit hücreleri (U937) boyut farklılıklarına göre uzaklaştırılarak meme kanseri hücrelerinin (MCF-7) yakalanması sağlanmıştır. Sonuçlar, burada geliştirilen yaklaşımların farklı alanlarda boyuta bağlı hücre ayrımı için mikroakışkan çalışmalara katkı sağlayabileceğini ortaya koymuştur.

TABLE OF CONTENTS

LIST OF FIGURES

Figures **Page**

Figures **Page**

ABBREVIATIONS

CTC	Circulating Tumor Cell
EMT	Epithelial-to-Mesenchymal Transition
MET	Mesenchymal-to-Epithelial Transition
FACS	Fluorescence-Activated Cell Sorting
MACS	Magnetically-Activated Cell Sorting
CBC	Complete Blood Count
RBC	Red Blood Cell
WBC	White Blood Cell
Hg	Hemoglobin
Hct	Hematocrit
SCD	Sickle Cell Disease
NRBCs	Nucleated Red Blood Cells
SLB	Support Lipid Bilayer
EPC	Epithelial CTCs
IMN	Immonumagnetic Nanosphere
EGFR	Epidermal Growth Factor Receptor
HER2	Human Epidermal Growth Factor Receptor 2
NP	Nanoparticle
DEP	Dielectrophoresis
DC	Direct Current
AC	Alternating Current
SAW	Surface Acoustic Wave
TSAW	Travelling Surface Acoustic Wave
SSAW	Standing Surface Acoustic Wave
FFF	Field-Flow Fractionation
DLD	Deterministic Lateral Displacement
PFF	Pinched Flow Fractionation
Gd	Gadavist

CHAPTER 1

INTRODUCTION

1.1. Concept of Cell Separation

Cell separation is used to separate homogeneous and individual cell classes from a heterogeneous cell population (Tomlinson et al. 2013). The efficiency and the purity of these separated cells are of great importance in personalized medicine, regenerative medicine, disease monitoring and drug testing as well as in the therapeutic and diagnostic researches (Bacon et al. 2020; Chin et al. 2020). Problems occur in cells create some alterations in the features of cells such as surface biomarker, density, size, weight, deformability and electrical properties and allow them to be distinguished from each other (Durmus et al. 2015). These features are applied in many areas of health. For example, early cancer markers circulating tumor cells (CTCs)can sed from the primary cancer site and circulate in the blood, can cause metastasis by spreading through different parts of a body, have great importance in the early diagnosis of cancer (Aghaamoo et al. 2015). Therefore, it is important to isolate CTCs from other cells but their low number in the blood makes it challenging (Bankó et al. 2019). Generally, antibodies specific to surface antigens of CTCs are selected to recognize them. However, it can be challenging to distinguish CTCs due to the different surface antigens of subclasses of CTCs and the changing of these antigens due to the epithelial-to-mesenchymal transition (EMT) and mesenchymal-to-epithelial transition (MET) processes (Ribatti, Tamma, and Annese 2020; Kasimir-Bauer et al. 2012). In addition, label-free separation methods provide the separation depending on the size, shape and deformability of CTCs (Hao et al. 2018). In clinical applications, the separation of blood cells provides benefits in much research, diagnosis and treatment methods (D. Lin et al. 2021; H. Zhang et al. 2021; Catarino et al. 2019). While erythrocytes and lymphocytes are used in the diagnosis of many diseases, mast cells and stem cells can also be used in determining the treatment methods (Thachil and Bates 2017). The diversities in physical properties of blood cells (size, shape, density) allow them to be identified from each other (Tomaiuolo 2014).

Another example of cell separation is the viable and non-viable cells used in cell culture, biomedical applications and cell transplantation (Chin et al. 2020). In this context, viable and non-viable cells can be differentiated from each other by using the characteristics of cells such as viscosity, stiffness, density and size (Islam et al. 2017). Separation of these cells is essential in cell transplantation in order not to stimulate the immune system (Tomlinson et al. 2013). Fluorescence microscopy and flow cytometry are mostly used to separate these cells although these methods damage the cells, increase the cost and can produce false-positive results (Marjanovič et al. 2014; McKinnon 2018).

The methods traditionally used to separate cells from each other are density, adherence, and antibody binding (Tomlinson et al. 2013). The adherence method can be used in cell culture. For example, stromal cells can be obtained and cultured by digesting the dental pulp enzymatically (Gronthos et al. 2000). Although this separation method is simple and inexpensive, it is non-specific and can be used where cell purity is not important. Density is one of the methods that is made by centrifugation and is routinely applied in laboratories. It is often used to separate mononuclear cells from the blood (Buckner et al. 1969). Although it is generally preferred in clinical, it can not specifically distinguish cell types that do not have a very different density from each other. Likewise, a method called a rosette using antibodies and density makes unwanted cells denser by labeling them with antibodies and forming a complex with erythrocytes. (Strelkauskas, Teodorescu, and Dray 1975). Then, by centrifugation, the unwanted cell complex precipitates and mononuclear cells are separated (Figure 1.1).

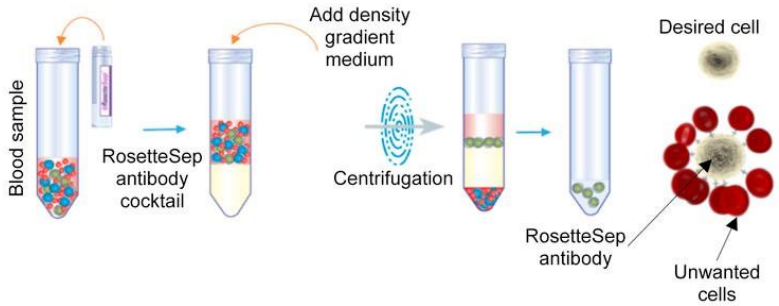

Figure 1.1. Rosette method for blood sample separation.
(Source: Rostami et al. 2019)

The methods using an antibody binding are generally Fluorescence-activated cell sorting (FACS) and Magnetic-activated cell sorting (MACS) (Xu et al. 2016). In the

FACS, antibodies conjugated with a fluorescent label are stimulated by a laser and send a signal to the cells (McKinnon 2018) (Figure 1.2. a). FACS is a desired method due to its sensitivity at a single cell level, high throughput of sorting and utilize multiple parameters (Bhagat et al. 2011). In the MACS, antibodies are conjugated with microbeads (Figure 1.2. b). Thus, unlabeled cells are removed under the magnetic field, while labeled cells are collected by removing magnets (Osman et al. 2013). Although MACS can not provide the individual cell separation, it requires the separation of microbeads from cells for the downstream process after separation. In the FACS, cell-specific separation can be achieved with a large number of antibodies, but this method takes hours while MACS takes 1 hour (Tomlinson et al. 2013). Immunoaffinity-based methods separate cells specifically by targeting their surface antigen using specific antibodies conjugated with a fluorescent label or magnetic particles (Bankó et al. 2019). The complex of antibody-magnetic beads causes unwanted cellular activities (Frenea-Robin and Marchalot 2022).

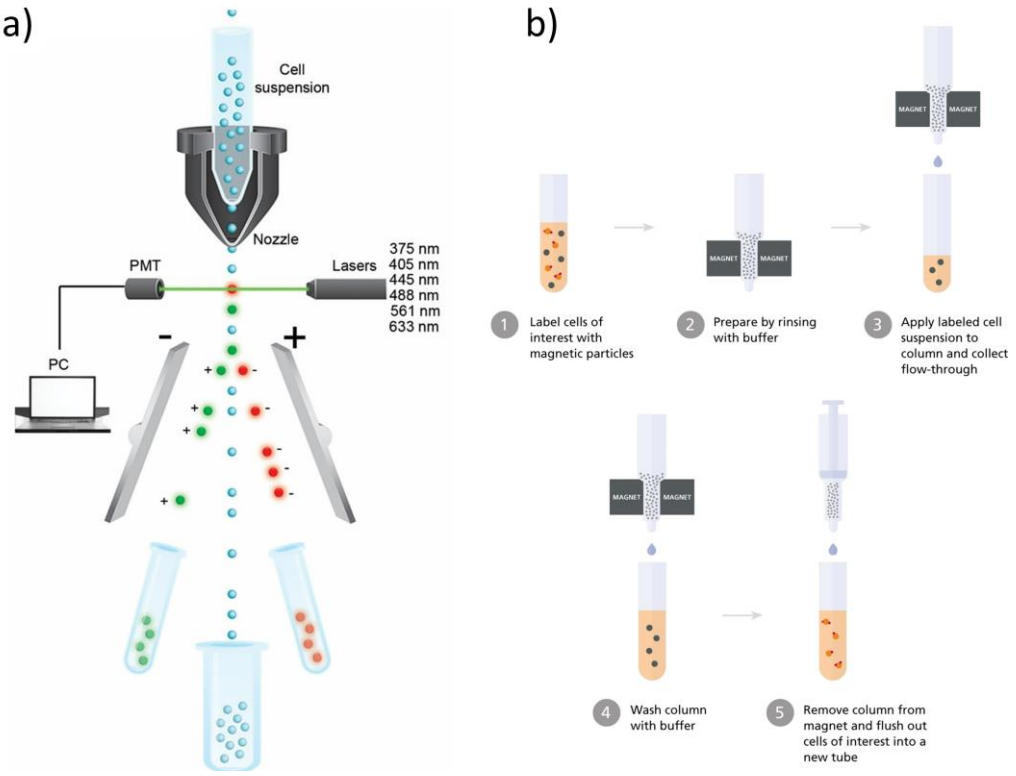

Figure 1.2. Cell separation techniques of FACs and MACS. (a) Fluorescently labelled antibodies are stimulated by a laser and gives signal depending on the cell characteristics at a single-cell level in FACS (b) Cells labelled with antibody conjugated microbeads and collected via magnetic field while undesired cells are removed in MACS. (Source: StemCell Technologies 2022; Hodne and Weltzien 2015)

1.2. Cell Separation in Clinical Perspective and Limitations of Conventional Cell Separation Methods

When blood cells become abnormal, they show different biological and physical properties from healthy cells (Durmus et al. 2015). This allows them to be distinguished in the clinic (Catarino et al. 2019). In blood tests, a complete blood count (CBC) is performed with red blood cell (RBC) level, white blood cell (WBC) and platelet level, hemoglobin (Hg) and hematocrit (Hct) measurements. The Hct value is the percentage of RBCs in the total blood and a low level of Hct indicates anemia (Mondal and Budh 2019). The Hct test is used in clinical and surgical applications. The centrifugation method is

used to separate the blood into its components (Basu and Kulkarni 2014). Thus, the blood is separated as RBCs at the bottom, WBC, platelet and plasma at the top (Figure 1.3. a). In the macro-hematocrit method, the blood sample is filled into the Wintrobe tube, then centrifugated at 3000 rpm for 30 minutes, the RBC height is controlled at the end (Mondal and Budh 2019) (Figure 1.3. b). In the micro-hematocrit method, the blood is filled into the capillary tube and both ends of the tube are sealed (Yang et al. 2001) (Figure 1.3. c). It is centrifugated at 11.000 – 12.000 rpm for 4-5 minutes and the results are controlled yang. The micro-hematocrit method is more useful in case blood sample collection is difficult. Automated analyzers measure the size and the number of RBCs based on the impedance as whole blood passes between two electrodes (Mondal and Budh 2019). Sickle cell disease (SCD) causes the deposition in RBC membranes and this increases the density and alterates the biophysical features of RBCs (Nader, Romana, and Connes 2020). It is known that increased RBC density is associated with hemolysis, ulcer and kidney failure (Connes et al. 2016). Recently, RBC density is measured by aqueous multiphase, arabinogalactan, density-gradient and phthalate density-distribution, however their applications are limited (Durmus et al. 2015). Nucleated RBCs (NRBCs) carry information about maternal, fetal and neonatal diseases (Davari-Tanha et al. 2014). The separation and sorting of NRBCs from pregnant women have been achieved by density-gradient separation, FACS, MACS and galactose-lectin methods (Wada and Kitagawa 2004). Due to the limited surface marker, these methods are limited. The separation of NRBCs with FACS presents low cell recovery and MACS presents low purity of cells (Wang et al. 2000). Recently, galactose-specific lectin is offered to separate NRBCs, however it is labor-intensive and causes contamination by non-nucleated RBCs (Huang et al. 2008). Malaria detection is made by parasite-infected RBC with density-gradient centrifugation since uninfected RBCs have distinct density (Trang et al. 2004).

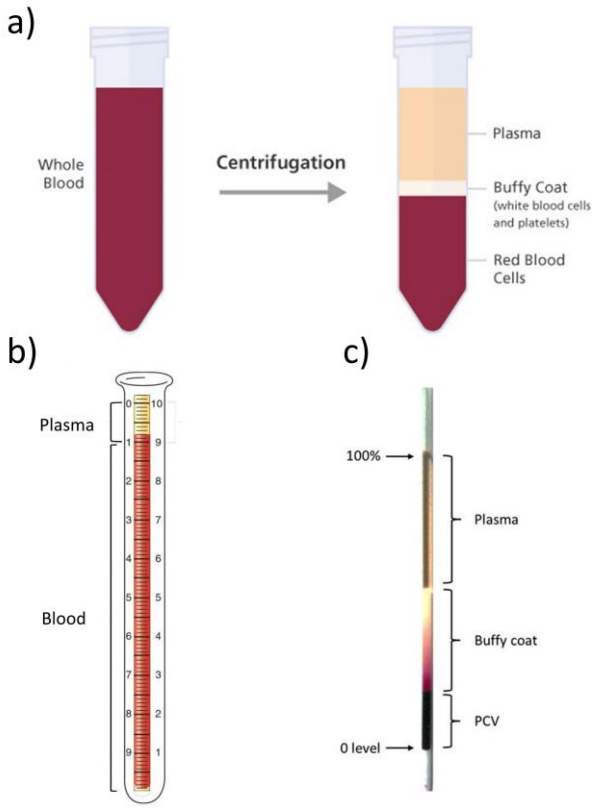

Figure 1.3. Hematocrit measurements. (a) Blood is separated into its components by the centrifugation. (b) Wintrobe tube filled with blood is centrifugated in macro-hematcorit method. (c) Capillary tube filled with blood and sealed at both ends is centrifugated. (Source: LaboratoryInfo, 2022; Novacco et al., 2015; StemCell, n.d.)

WBC count in the normal blood is 4.000 – 10.000 per µl and is usually made by special chambers and automated counters (Blumenreich 1990). It can be examined morphologically by smear and staining on glass slides to identify different classes (Jaebum Chung et al. 2015). Accurate counting and discrimination are difficult with these methods. Looking at subclasses of WBCs, an underproduction of granulocytes causes neutropenia, while eosinophils are associated with parasitic infection and pulmonary infiltrates (Tvedten and Raskin 2012). Basophils are the key classes of myeloproliferative disorders, some chronic inflammatory and infectious diseases (Blumenreich 1990). Evaluating the leukocyte number and differences within the scope of CBC, diagnosis of inflammation, leukemia and immunodeficency can be performed (Hamad and Mangla 2019). While the abnormal platelet count is associated with diseases such as lymphoma

and aplastic anemia, a diagnosis of bleeding, anemia and cancer can be made by examining the RBC count (Thachil and Bates 2017). In commercial systems using optical and electrical approaches, the blood is divided into two channels (Hassan et al. 2015). In optical analyzers, cells are illuminated by the laser. The scattered light is called the forward scatter light and the light collected by the photodetector is called the backscatter light (MacCallum, Cunningham, and McKee 2004). These ensure the information about the dimension of cells and membrane proteins. Electrical analyzers give dimensional and membrane protein informations of cells in the blood with electrodes with frequencies in different ranges (Hassan et al. 2015).

A cancer diagnosis can be made by diagnostic imaging techniques, biomarker tests and biopsy (Dommett et al. 2012). Tumor cells are taken from the tumor site and analyzed in pathology (Gold and Cankovic 2015). However, a biopsy can create unwanted situations for the patients since it is an invasive method (Alieva, van Rheenen, and Broekman 2018). There are several technologies for the detection of CTCs in the blood based on their physical or biological properties (Ferreira, Ramani, and Jeffrey 2016; Toss et al. 2014). CTCs can also be separated from blood with centrifugation using density differences between CTCs and blood cells (Bankó et al. 2019). Immunoaffinity-based methods are one of the most used methods for CTC, providing recognition with antibodies specific to antigens on the cell surface. Tumor cells have different surface markers from blood cells such as EpCAM, cytokeratin (CK) and are differentiated in blood by these markers (habli). However, this can be misleading due to the dynamic expression of EpCAM according to the origin of CTCs and stages of different cancers (Gires and Stoecklein 2014; Habli et al. 2020).

1.3. Microfluidic Cell Separation Methods

Conventional methods are widely used in clinical laboratories, diagnostic tests and research (Bunn and Sikarwar 2016). However, the limitations of conventional methods applied as routine tests in hospitals carried out by bulky and costly devices and technical personnel (Armbruster, Overcash, and Reyes 2014). Also, the results take a long time, protocols include complex steps and errors can be created by pipetting or human intervention. Microfluidic systems have been developed to solve problems encountered in conventional methods and to present similar principles in micron-size (Shields IV,

Reyes, and López 2015). Recent microfluidic systems are divided as label-based and label-free methods (Figure 1.4.).

Label-based methods are applied using the affinity approach either functionalizing the microfluidic surface with specific antibodies/aptamers or these antibodies can be conjugated with fluorescent labels or magnetic particles (Bankó et al. 2019). On the contrary, label-free methods do not require labels as they utilize physical properties for the separation. Label-free microfluidic systems are divided as whether external force is applied (active) or not (passive). Active systems apply forces such as acoustic, electric, magnetic and optical. Passive systems utilize structures and inertial forces (Shields IV, Reyes, and López 2015). Hybrid methods that combine active and passive approaches are implemented to enhance separation efficiency. Microfluidics systems have several advantages such as reducing the size and cost, low consumption of sample and reagent and eliminating complex devices and protocols (Shields IV, Reyes, and López 2015) When microfluidics are compared to the conventional methods, they offer parallel tests and consider multiple parameters and minimize the contamination and safety problems (Jayamohan, Sant, and Gale 2013).

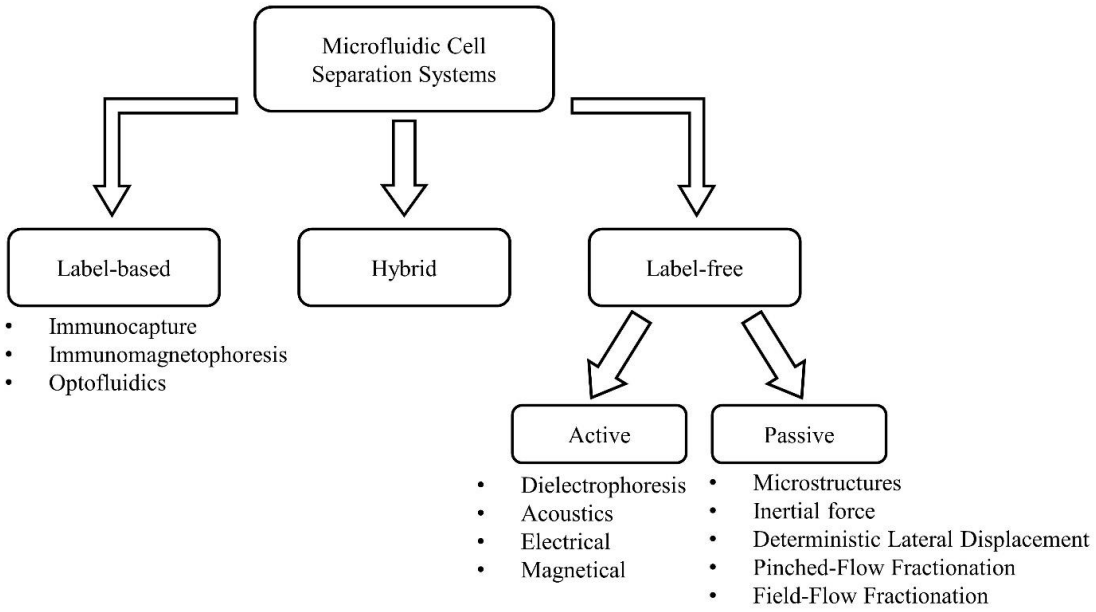

Figure 1.4. Microfluidic cell separation methods as label-based, label-free and hybrid.

1.3.1. Label-based Methods

Label-based separation of cells includes immunocapture and immunomagnetophoresis in microfluidic systems (Cho et al. 2018). Microfluidic surfaces or microfilter structures can be functionalized with specific antibodies to enhance cell attachments in immunocapture techniques (Tian et al. 2018) (Figure 1.5. a), while magnetic nano/microparticles can be functionalized using antibodies or aptamers in immunomagnetophoresis separation techniques (Cho et al. 2018) (Figure 1.5. b).

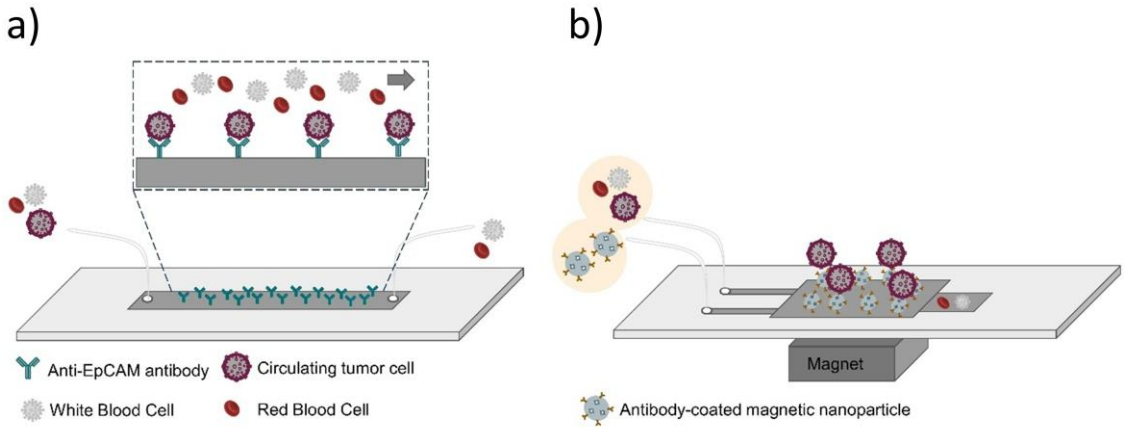

Figure 1.5. Label-based cell separation demonstrated in CTC capturing. (a) Microfluidic surface is functionalized with antibodies targeting surface antigens of CTCs. CTCs are captured and other blood cells are washed away. (b) Magnetic microparticles functionalized with tumor-specific antibodies are kept with magnets. CTCs are captured with microparticles and by removing the magnets, CTCs can be collected.

Microfluidic device coated with Anti-EpCAM antibody was used for the isolation of CTCs from blood samples (J. Chen et al. 2020). The surface of microfluidic was functionalized with the help of self-polymerized dopamine and streptavidin-biotin interactions. EpCAM positive breast cancer, colon cancer and prostate cancer cell lines and EpCAM negative kidney cancer cell lines were used and capture efficiency was found as 92.42%, 87.74% and 89.35%, respectively. Antibody conjugated support lipid bilayer (SLB) coating was presented to capture CTCs and circulating tumor microemboli (CTM)

from all-stage clinical cancer patients' whole blood (J.-Y. Chen et al. 2016). The non-fouling property of SLB provides interaction between an antibody and CTC antigen by decreasing the retention of blood cells with the flow. Viable CTCs were released by giving a stream of air foam to breakdown the SLB structure. The 95% releasing efficiency was obtained and it was found that at least 86% of recovered cells keep their viability. This study was shown high detection rates for the first time and achieved quantification of non-metastatic CTCs. Automated microfluidic chip-based CTC detection was used for SKOV3 ovarian cancer cell line (Jou et al. 2021). To evaluate CTC capture efficiency in peripheral blood, healthy volunteers and patients with ovarian tumors and epithelial ovarian cancer were used. For spiking test in an ovarian cancer cell, capture rates were found as 48.3% using only anti-EpCAM and 89.6% for the combination of anti-N-cadherin. With this device, CTCs can be captured, identified, enumerated and characterized on-chip. Carpet chip including antibody-coated micropost structure, targeted EpCAM+ CTCs and CD133 to capture pancreatic stem cells and CTCs (Zeinali et al. 2018). Two devices coated with anti-EpCAM and anti-CD133 were connected and blood was given to the inlet of one device with a 1 mL/h flow rate. From pancreatic cancer patients, epithelial CTCs (EPCs) and epithelial-to-mesenchymal transition (EMT)-like CTCs (EMTCs) were detected simultaneously with above 97% efficiency and 76% purity. The authors stated that the system has the potential for diagnostic and therapeutic applications for cancer. Amicrofluidic device containing the micropillar surface was immobilized with aptamer and used to isolate tumor cells from whole blood (Sheng et al. 2012). Aptamers were immobilized with the avidin-coated micropillar surface and captured CTCs from their surface receptor. Approximately, 95% capture efficiency and 81% purity were obtained with a flow rate of 600 nL/s. The device can isolate 10 colorectal tumor cells from 1 mL of whole blood in 28 minutes.

Immunomagnetic microfluidic device was presented to separate CTCs (Tang et al. 2016). Microfluidic device consisted of three layers; first layer containing the channel for sample processing and immunomagnetic nanosphere (IMN) pattern formation. Middle layer was made of glass containing Nickel patterns to increase local magnetic field for capturing of magnetic beads. IMNs were loaded into device with magnets and created patterns due to increased local magnetic field with patterned nickel. It was observed that IMN patterns stayed the same after the experiment and the capture efficiency of this system reached up to 94% from the bloodstream. Captured cells were collected by removing permanent magnets. Immunomagnetic CTC separation achieved the

combination of the micro-magnet array provided with inkjet printing and the external magnetic field with permanent magnets (P. Chen et al. 2016). The whole blood sample was mixed with anti-EpCAM coated magnetic nanoparticle suspension. Cancer cells were separated magnetically, RBC and WBCs removed along with blood sample flows. The capture rate was 26% increased with inkjet micromagnet structure. A microfluidic platform was presented using spectrally combined encoding and multifunctional nanospheres by targeting different biomarkers (EpCAM, EGFR, HER2) labeled by nanosphere barcodes that have special magnetic tags and optical signatures (L. Wu et al. 2020). When this system integrated with their on-chip single-cell fluorescence detection platform (L.-L. Wu et al. 2018), CTCs were trapped on microstructures. This technology provides profiling of CTCs for precision medicine. A microfluidic system including biomimetic nanoparticles (NPs) was presented for the CTC detection. Membrane fragments of leukocyte were used to camouflage magnetic nanoclusters and EpCAM-specific aptamer were used for CTC detection (F. Zhang et al. 2019). Nanoclusters were magnetically loaded into the device and aptamer integrated magnetic nanoclusters were arranged in nickel patterns. With this system, leukocyte adsorption is eliminated using leukocyte membrane fragments and 90% of CTCs in the blood can be captured in 20 minutes.

1.3.2. Label-free Methods

Label-free methods can separate cells by their size, density, deformability and electrical charges and they can be adapted to microfluidic system by controlling geometry and fluid flow (Fu et al. 2021). Label-free methods are divided into active and passive according to whether external force is used or not.

1.3.2.1. Active Methods

Active microfluidic separation approaches require external forces such as electrical, acoustic and magnetical to separate cells by their properties. Since cells possess different dielectric properties, efficient separation of cells can be obtained by creating an electrical field in the dielectrophoresis (DEP) (Gascoyne et al., 2013). DEP can be described as the movement of cells within a non-uniform electrical field according to their

dielectric properties (Shields IV, Reyes, and López 2015). Harming of cells due to the Joule heating or separation problem of cells that have similar dielectric properties are pitfalls of DEP (Farahinia, Zhang, and Badea 2021). Direct current (DC) DEP cell sorter was presented to achieve separation of yeast cells, 4T1 tumor cells and bone marrow cells of murine (J. Sun et al. 2012). The cells were compressed by the flow towards the triangular barrier. When cells were subjected to a strong DEP force, they were pushed away from the barrier by the negative DEP force. Since the large cells were subjected to greated DEP, they were pushed farther than small cells. Finally, cells at different distances diverged into different branches. Their system reduced the exposure of cells to the electrical field. Multiple DEP force by changing the electric field in a microfluidic device was presented for the stem cell sorting (Song et al. 2015). The system contained two inlets for the cell mixture and the buffer solution. DEP was generated by interdigitated electrodes by changing the AC field. Strong DEP force was applied to osteoblasts deflected zig-zag while the human mesenchymal stem cells experienced weak DEP stayed their trajectory. According to the results, human mesenchymal stem cells were collected with 92% efficiency and osteoblasts with 67%. An AC-DEP microfluidic system containing two-electrode pads on the sidewalls of microfluidic was designed to create a non-uniform electrical field (Zhao et al. 2019). When the cells exposed a positive DEP force were moved through the electrical gradient, cells were repulsed due to the negative DEP force. The separation of dead and live yeast cells was examined by changing the frequency and AC-electric field by considering the size and dielectric properties of the cells. As a result, live and dead yeast cells experienced different DEP forces between 1.7×10^6 Hz – 4.3×10^7 Hz.

Acoustic force is manipulated cells with standing waves over the microfluidics (P. Zhang et al. 2020). Depending of the size, density and compressibility, the distance of movement varies between cells. The integrity and functionality of cells have been shown by the surface acoustic wave (SAW) which is classified as traveling SAW (TSAW) and standing SAW (SSAW). Acoustic force is adjusted in TSAW and optimizes the sorting rate. On the contrary, SSAW provides fixed wavelength and high throughput (Shen, Yalikun, and Tanaka 2019). Tilted-angle SSAW was examined on polystyrene beads with different diameters with 99% efficiency and showed the efficient separation even in the same properties of cells that differ in compressibility (Ding et al. 2014). The system utilized the inclined angle positioned pressure nodal lines to the direction of flow. With this angle, a particle exposed to acoustic radiation force and laminar drag force. Thus, a

particle took longer distance compared to traditional methods. The separation efficiency was enhanced both with the inclined angle and the multiple nodal lines that captured the target particles better. The separation of small particles succeeded while they were repulsed by the flow field as they were exposed to small acoustic force. Besides, the tilted-angle SSAW approach was separated the MCF-7 breast cancer cells from WBCs with a 71% recovery rate and 84% purity.

The magnetic field is created by magnets in microfluidic systems and cells placed in paramagnetic or ferrofluidic solutions are demagnetized (Figure 1.6. a) (Yaman et al. 2018). Placing the first magnet close to the channel and the second magnet far from the channel provided continuous alignment of particles (Zeng et al. 2013). 3 μm and 10 μm polystyrene particles were separated to model live yeast cells. The phenomenon of particles suspended in a paramagnetic environment under a nonhomogeneous magnetic field is magnetic levitation (Yaman et al. 2018). The height at which the particles levitate under the magnetic field depends on the magnetic susceptibility and density difference of the medium and the particle. This method is used for cell detection, biomarker detection and material characterization. The magnetic levitation principle was utilized with a significant resolution for the separation of breast, esophageal, colorectal and non-small cell lung cancer cell lines (Figure 1.6. b) (Durmus et al. 2015). According to density differences of cell lines, cells were levitated at their specific position. The same principle was offered using two opposing magnets with a capillary channel (Delikoyun et al. 2021). In this system, the levitation height of dead and live bone marrow stem cells was examined and dead cells can be collected at low levitation heights (Figure 1.6. c).

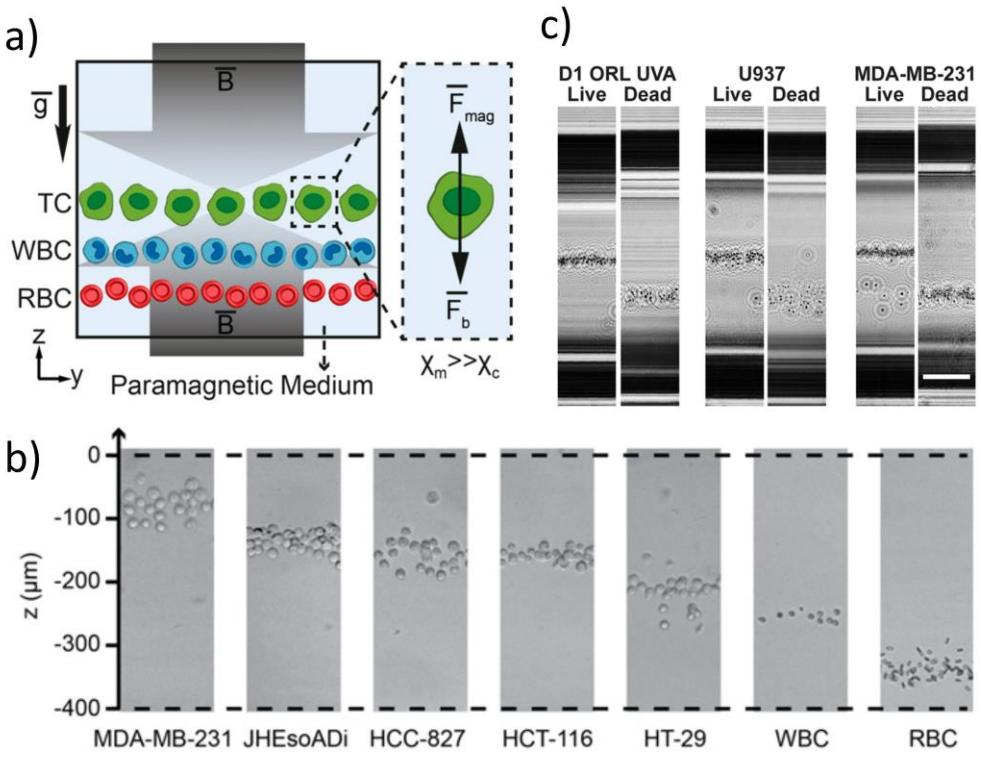

Figure 1.6. Magnetic levitation principle for cell separation. (a) The magnetic field created by magnets in microfluidic systems and cells are levitated. (b) The magnetic levitation principle for the separation of breast, esophageal, colorectal and non-small cell lung cancer cell lines. (c) Different levitation heights of dead and live bone marrow stem cells. (Source: (Delikoyun et al., 2021; Durmus et al., 2015).

1.3.2.2. Passive Methods

Passive microfluidic approaches do not require external forces other than hydrodynamic forces to separate cells (Shields IV, Reyes, and López 2015). Microstructures are physical structures containing weir-type filters, pillars and membranes. Generally, these barriers are designed to trap desired cells with a specified size and undesired cells pass with the flow (Warkiani et al. 2015). A weir-type microfluidic system was utilized to separate tumor cells according to their size (Jaehoon Chung et al. 2012). The system contains sample inlets, a separation channel with weir structure and collection outlets. Small cells were directed to their port by passing through the gap, while large human A431 cancer cells flew along the barrier and collected with a

>95% recovery at 20 mL/h. A membrane structure with multilayer lateral flow was used for the filtration of SK-BR-3 cancer cells with a 93% recovery rate (Jiang et al. 2018). The system composed of a first layer as parallel microchannels that contain inlets and outlets, a second layer contains porous membrane and a third layer has cylinder pillars. Larger particles did not pass from the membrane and moved to the outlet at the top layer. Smaller particles were separated with the lateral flow. Another geometry is micro-sieving (μ-sieving), which overcomes clogging of cells during continuous flow with mechanical oscillation having 130 Hz frequency (Yoon et al. 2016). Firstly, polystyrene particles having 5 μm and 20 μm diameters were separated with 100% efficiency. Afterward, breast cancer cells (MDA-MB-231) were separated from whole blood with the same procedure with polystyrene microparticles. The fabricated μ-sieving filter device prevents blood coagulation and cell loss. The utilization of microfilter structures was limited due to the clogging and deformation of structures, low purity of collected sample because of the filtration of unwanted cells (Alvankarian, Bahadorimehr, and Yeop Majlis 2013).

Field-flow fractionation (FFF) separates cells according to their size and morphology using inertial or non-inertial forces. FFF microfluidic approaches possess multiple channels for the separation allowing on-chip sample processing (Sant and Gale 2007). The separation of particles is performed with the displacement of a particle with the flow and the properties of a particle affect the retention time in the channel (Williams, Runyon, and Ashames 2011). Generally, FFF is applied combined with other techniques such as DEP, magnetic, acoustic and sedimentation.

Particles displace perpendicular to flow in deterministic lateral displacement (DLD) (Gossett et al. 2010). Critical diameter is determined for the displacement of suspended particles for a system (Aghilinejad, Aghaamoo, and Chen 2019). A zigzag pattern without lateral displacement was observed in any particles with a diameter less than the critical diameter. Particles with greater diameter will cross streamlines and lateral displacement observed (Okano et al. 2015). DLD-connected inertial microfluidic called I-DLD sorter operated with two stages (Xiang et al. 2019). In the first stage, removal of other blood cells was achieved using spiral inertial microfluidic. In the second stage, the DLD sorter with a triangular post removed the remaining blood cells. 100% separation was completed for the separation of microparticles with 15 and 7 μm. In the first stage, 96.31% of blood cells were removed and in the second stage, 3.63% of blood cells were eliminated. Recovery of tumor cells was obtained with 91.34%. Deformability and size-based separation of CTC was achieved in a microfluidic chip with two integrated

modules; one with mirrored DLD array for blood cell depletion according to size and the other with tilted angle DLD array for deformability and size-based separation (Liu et al. 2018). In the system, RBCs moved with the flow, WBCs and CTCs moved through the tilted micropost array. While CTCs were moving with a tilted array, WBCs followed the direction of the fluid. Blood cells and CTCs were collected from different outlets. The system can process the continuous sample with >90% capture efficiency and >50% purity at 12 mL/h. The separation of viable and non-viable mammalian cells with a DLD microfluidic system was achieved by referring to the size differences between apoptotic cells and normal cells (Tottori et al. 2016). The system includes two inlets for the sample solution and the other for the buffer solution to expose cells to hydrodynamic force and direct them through sidewalls. In this regard, viable Jurkat cells were separated from nonviable apoptotic cells with 100 % efficiency and 23.1% purity at a 20 μm gap, and the capture efficiency and purity were founded as 48.2% and 50.2%, respectively, at a 23 μm gap.

Pinched flow fractionation generates pinched segments from suspended particles and aligned them using another flow without particles (Yamada, Nakashima, and Seki 2004). PFF size-based separation system was used for the separation of LS174T colon cancer cells from WBCs (Pødenphant et al. 2015).Samples with particles of different sizes and carrier solutions were given into different inlets. When they meet a narrow channel, a pinched segment was created and particles were aligned against the sidewall of a channel. The pinched segment was deviated into small, large and drain channel outlets. 90% efficiency which is the highest efficiency for this system was obtained at a 10 μL/h flow rate. A combination of elastic and inertial lift forces (elasto-inertial PFF) showed the separation of particles of smaller size (Lu and Xuan 2015). First, particles were aligned against on sidewall and due to the steric effect, larger particles were located far from the wall. It was stated that their work has the potential to separate very small particles. Microalgae separation was used in an inertia-enhanced PFF system (Y.-H. Lin et al. 2013). The microfluidic system contained two inlets, one outlet, two side branch channels and the main channel. According to the study, separation was increased with increasing Reynold's number but reached saturation then. Separation recoveries of *Tetraselmis* sp. and *Chlorel*la sp. founded as 90% and 99%, while their purities were 86% and 99%, respectively. The same principle was applied to separate viruses and spermatozoa in semen samples (Hamacher et al. 2021). Two parallel inlets for the buffer and sample associated with the pinched segment were designed. While the viruses moved close to the

wall of the channel through one outlet, spermatozoa moved with the streamlines and collected from another outlet. 84% removal of viruses and 86% recovery of spermatozoa was achieved by using a significantly large size difference of spermatozoa than the virus.

1.4. Centrifugal Microfluidic Systems in Cellular Applications

Isolation from a sample with high purity, high viability and good yield is the most important step of any research (Al-Faqheri et al. 2017). In this context, centrifugal microfluidic systems offer simple and multifunctional approaches to diagnostic and clinical testing (Hugo et al. 2014). Implementing features such as mixing, droplet formation and flow profiling are the advantages of centrifugal microfluidic systems over other microfluidic systems (Clime et al. 2019). Traditionally, applications such as centrifugation, sedimentation, cell separation and enrichment are achieved preventing contamination regardless of the sample's viscosity, electrical conductivity and pH faqheri.In particular, centrifugal microfluidic systems eliminate structures such as pumps and active valves, eliminating off-chip sample processing and error-prone pipetting (Hugo et al. 2014). In lab-on-a-cd platforms, the force applied by the rotation effect is the centrifugal force (Fcen), and pressure is applied to the fluid with this force (Al-Faqheri et al. 2017)

$$Fcen = \rho \times \omega^2 \times r \qquad (1.1)$$

,where ρ is the density of a fluid, ω is the rotation speed (rad/s) and r is the distance of a fluid from CD center.

Capillary valves located in lab-on-a-cd structures create a sudden opening with the effect of centrifugal force, while the liquid flows with the effect of centrifugation, the capillary force applies pressure in the opposite direction (Pcap).

$$Pcap = \frac{4 \cos \theta c \, \gamma la}{Dh} \qquad (1.2)$$

where θc is the surface contact angle of a fluid, γla is the surface energy of fluid-air and the Dh is the hydraulic diameter.

For the liquid to pass through the valve and reach the flow profile, the centrifugal pressure must be greater than the capillary pressure, otherwise, no flow will be observed in the balance of these two forces. In addition, there is the Coriolis force (Fcor) perpendicular to the direction of movement, acting on the rotating platforms under the centrifugal effect, and the Euler force (Fe), which is encountered in curved microchannels, which supports the centrifugal force (Al-Faqheri et al. 2017):

$$\mathrm{Fcor} = 2 \times \rho \times \omega \times \mathrm{U} \tag{1.3}$$

with U the average velocity of a fluid and

$$\mathrm{Fe} = \rho \times \mathrm{r} \times \frac{\mathrm{d}\omega}{\mathrm{dt}} \tag{1.4}$$

The structures used in centrifugal microfluidic structures are divided into passive and active. While passive structures are made by a capillary valve, siphon valve and Coriolis valve that do not require moving parts or external force, active structures are structures such as pinch valve and wax valve that need moving parts and external forces to create flow (Clime et al. 2019).

Filling, addition and mixing of a sample in a microfluidic disc are shown in the system consisting of the upper layer containing the sample and air inlets, the middle layer including the chambers and the lower layer containing the channels (Al-Faqheri et al. 2017). With the application of the centrifugal force, the liquids in the chamber begin to be compressed and with the subsequent increase in the applied force, the capillary force weakens and the first solution flows into the chamber. By increasing the centrifugal force, the second solution also flows into the chamber and combines with the first solution. The pumping method, which allows the fluid to move back and forth in the channel, depending on the dominance of the capillary force by increasing or decreasing the centrifugal force, is presented (Clime et al. 2019). The system requires a liquid-solid interface and some of the liquid stayed in the chamber. So, this system can be applied to increase efficiency as a supplement system. A study that pumps fluids radially inward was carried out using a high-density fluid, under the centrifugal force, would push a less dense sample fluid towards the center of rotation (Kong, Bouchard, and Salin 2012). Immiscible liquids or

air as the intermediate phase are needed to maintain sample integrity. Its unidirectional character and the need for an additional fluid for pumping limit this approach. A presented passive pumping system incorporates a principle based on the pneumatic air compression by hydrostatic pressure generated in the fluid branch in an adjacent channel. In this study, fluid was pumped back to the center by releasing the stored pneumatic energy by reducing the rotation speed (Clime et al. 2019). Although the method is precise and reproducible, it requires the fabrication of additional compression chambers. In a centrifuge system using a siphon valve, the siphon structure can discharge fluids within a rotational speed range or stop the flow by increasing the rotation frequency (Zhu, Chen, and Xu 2018). The intermittent siphon valve consists of an additional air hole at the top of the siphon. When the rotation is stopped, the siphon is fed, and when the rotation of disc starts and reach the enough speed, the liquid in the siphon conveys away from the center. Thus, air will move through the siphon from the air hole at the top of the siphon and stop the liquid in the siphon channel. At the lower rotational speed, it forms a meniscus at the gas-liquid interface. The liquid is conveyed from the charging chamber to the collection chamber via the siphon. The design and fabrication of centrifugal systems containing siphon structures are complex.

A centrifugal microfluidic platform offered density-gradient separation of peripheral blood mononuclear cells (PBMCs) from whole blood were achieved (Y. Sun and Sethu 2018). The blood and Ficoll tubings were filled into the reservoir and then flow into the spiral channel by centrifugal force and the cells in the channel were exposed to a drag force. Since the RBCs are polymorphonuclear cells heavy, the centrifugal force acting on th is greater than the buoyancy force, and while the cells move towards the wall, the buoyancy force acting on the PBMCs overcome the centrifugal force and remains at the interface. A centrifugal microfluidic system including an aqueous two-phase for cell isolation from whole blood and active pneumatic pumping for the flow of fluids has been developed (Figure 1.7. a) (Moon et al. 2021). A mixture of polyethylene glycol (PEG) and dextran (DEX) was used for cells of different densities. After a centrifugation, layers consisted of high density-gradient medium, RBCs, neutrophils in DEX layer, buffy coat and plasma from bottom to top. It has been shown that each layer formed can be collected into separate tubes with >90% cell viability. A centrifugal disc can separate serum from blood with a system compatible with hydrophilic and hydrophobic biomarkers, the cross-flow filtration method, separated the serum and retained the amphiphilic biomarkers in the serum (Figure 1.7. b) (Lenz et al. 2021).The device consisted of chambers located one

above the other, separated by a membrane, and there were four separation units on the disc with different functions. During cross-flow filtration, the sample passed tangentially through the filter by centrifugal force. As the pressure increases, components smaller than the pores of the membrane passed through the filter, while larger components passed through the surface of the membrane. In a study using an active pumping element, there was a pump system closed with deformable polymer layers by integrating permanent magnets on the system (Haeberle and Zengerle 2007). A constant flow of liquid was started by compressing the air in the deformable chambers by allowing the chambers to rotate in a constant magnetic field. Although active element centrifugal microfluidic systems offer interesting methods, their implementation requires equipments that must be mounted on the rotating platform and their control. In a centrifugal platform built by integrating electronic pumps and using electromechanical valves, the platform rotated at high speed and created air pressure at the pressure ports on the chip via a pneumatic connection (Clime et al., 2019). The resulting air pressure interacted with the circuit elements and performed functions such as valving, reverse pumping and a bubble mixing. Also, the cost such a complex platform is also increasing.

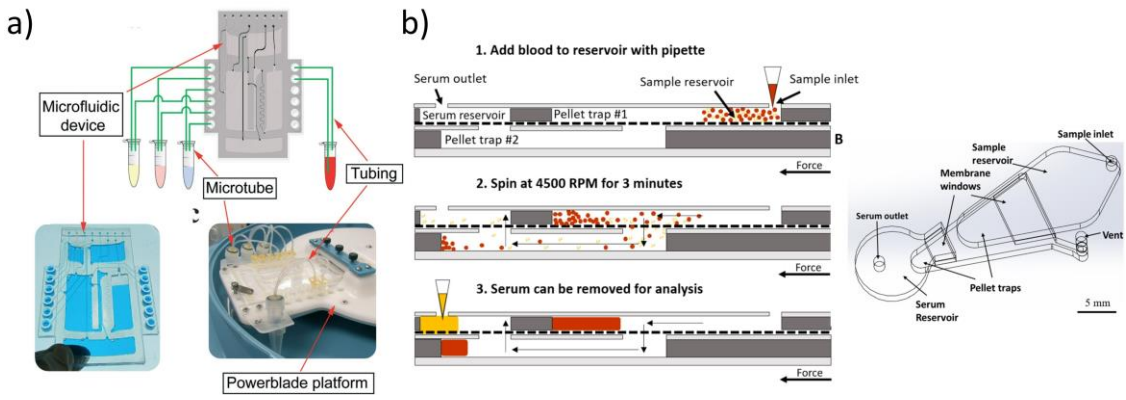

Figure. 1.7. Centrifugal microfluidic applications. (a) Powerblade platform suitable with centrifugation (b) Centrifugal disc can separate serum from blood with a system compatible with hydrophilic and hydrophobic biomarkers. (Source: (Moon et al. 2021; Lenz et al. 2021)).

1.5. Blood Sample Manipulations in Microfluidic Systems

Alterations in blood rheology such as the viscosity of blood and plasma, deformation of RBC are the significant signs of diseases and vital for the diagnosis in clinical (Pinho et al. 2020). The ability of CTCs to circulate in the blood, which has great importance in the diagnosis of cancer, has also made it possible to analyze this important marker by separating it from the blood (Bankó et al. 2019). Electrical properties, impedance differences or physical distinctions of blood cells have been used in microfluidics to achieve separation with low sample volume without complex and painful techniques (Pinho et al., 2020).

A partial CBC from 10 μL of blood was achieved in a microfluidic system where RBCs lysed on-chip and leukocytes were counted electrically (Hassan et al. 2015). The gaps of platinum electrodes were determined as a minimum of 15 μm since granulocytes and monocytes have 12-15 μm. Pulses were related to the size of cells and 65% recovery of WBCs was obtained whereas platelet count efficiency was low as 50-60%. Two-stage separation of WBCs labeled with immunomagnetic micro/nanoparticles (IMNPs) suggested the lateral and vertical magnetic forces (S. Lin et al. 2019). A lateral magnetic stage composed of nickel microarray was used to enrich cells and a vertical magnetic stage was used to lift target cells and remove undesired cells where Drag force is dominated. According to the results, 93% separation purity and 97.5% viability of WBCs were obtained at 20 μL/min. Another blood study for the extraction of plasma, RBC and capturing of WBC was obtained in an integrated cross-flow and hydrodynamic flow microfluidic device (Kuan et al. 2018). The device was composed of inlets for whole blood and buffer, a bifurcation region and three zones. Only plasma flowed through its zone at first and due to the deformability of RBCs, they were collected from their zone. Then, WBCs were trapped in the pillar structure of the channel. It was shown that this system can capture approximately 1,800 WBC in 20 minutes and plasma, RBC and WBC can be collected from 6 μL samples, simultaneously. WBC separation with a 72.1% recovery rate was obtained using a bidirectional micropump to prevent clogging and commercial polycarbonate microporous membrane to pass RBCs (Cheng et al. 2016). RBCs and platelets were filtered in a microporous membrane which separates two microfluidic chambers, while the WBCs moved to the filtration region. By working the motors reversely, cells collected in micropores were moved back to prevent clogging.

Blood plasma was turned into paramagnetic condition using superparamagnetic iron oxide nanoparticles (SPIONs) in a microfluidic diamagnetic approach (Kwon et al. 2021). Magnetic flux density was enhanced with Halbach magnetic array. Blood cells were moved to the bottom of the channel due to the diamagnetic forces and 83.3% recovery of plasma was collected from 4 mL of a blood sample. In a continuous flow microfluidic system, large WBCs were separated with Dean flow force and inertial migration with a 93.3% and smaller RBCs removed hydrodynamic suction found 0.1% in collected cells (Lombodorj et al. 2020). A blood sample was moved through the connected curve channel where the RBCs were kept in the channel and WBCs were moved towards. Human blood labeled with fluorochrome-conjugated monoclonal antibodies in the microfluidic system contains DLD and micropost array (Civin et al. 2016). 88% WBC recovery, 99.9% RBC and unbound monoclonal antibody removal were shown in 18 minutes. Smaller cells (RBCs, platelets) moved through micropost array whereas WBCs were pushed through the outlet. A magnetic device was designed to examine the density and magnetic susceptibility difference between uninfected RBCs and Plasmodium falciparum-infected RBCs (Deshmukh et al. 2021). Fingerprick blood and paramagnetic solution were mixed and loaded into the capillary and a magnetic device. The system reached equilibrium in about 12 minutes. The infection of RBCs made changes such as increment in magnetic susceptibility and decrement in density which increase the buoyancy force and decrease the gravity and magnetic repulsion force. As a result, infected RBCs levitated higher in a channel. With the same magnetic principle, by taking advantage of the density difference of the RBCs, polymorphonuclear leukocytes and lymphocytes and RBCs by age were separated in a magnetic platform each cell type has its levitation height (Tasoglu et al. 2015).

Since the CTCs and blood cells have different sizes from each other, hydrodynamic approaches including the inertial lift force and Dean force were used to separate them (Lee et al. 2013). With this regard, a microfluidic system with an array of contraction-expansion was applied to separate cancer cells at a low Reynolds number to eliminate high shear stress. Fluid coming from the contraction array was accelerated in the expansion region. In a channel, inertial lift force affected the cancer cells and move away from the center of the channel, while inertial lift forces dominated the small blood cells with the Dean drag force moving through the sidewall. With this system, 99.1% of cancer cells (MCF-7, SK-BR-3, HCC70) were recovered from whole blood with a throughput of $1.1x10^8$ cells/min. Utilizing the same approach of inertial lift force and

Dean drag force, size-based separation of large HeLa cells was achieved with >90% efficiency at $2.6x10^8$ cells/min throughput in a double spiral channel (J. Sun et al. 2013). Size-based separation of tumor cells from whole blood was achieved in an interfacial viscoelastic microfluidic system (Tian et al. 2018). Tumor cells were penetrating with sample and viscoelastic flow while blood cells were blocked with inertial lift forces and interfacial elastic lift forces. It was shown that the viability of tumor cells was protected 100% after separation with 95.1% efficiency at 50 tumor cells/mL. Since the WBCs and CTCs have similar sizes, hybrid approaches can enhance cell separation (Nasiri et al. 2020). In this system, MCF-7 cells were conjugated with EpCAM antibodies and magnetic nanoparticles to increase the magnetic susceptibility of cells. In the first stage, RBCs and WBCs were removed in an asymmetric serpentine channel with inertial lift force and Dean drag force. While the RBCs and WBCs were directed to the sidewalls, CTCs were moved to the middle of the channel. In the second stage, the magnetic cell separator eliminated the WBC impurities with 93% efficiency and 95% recovery of CTCs.

A spiral channel microfluidic system achieved 90% recovery of sperm cells and 89% and 74% removal of RBCs and WBCs, respectively (Nepal, Feng, and Gale 2020). Shape and size-based separation of sperm cells were observed by moving them far from the inner channel wall where the inertial lift force is dominated, while the blood cells move through there.

CHAPTER 2

VACUUM-INTEGRATED MICROFLUIDIC CHIP

2.1. Background

Polydimethylsiloxane (PDMS), which is the basic material of microfluidics, is frequently used in microfluidics due to its gas permeability, easy bonding, transparency and low cost. The air permeability feature of PDMS has an ideal utilization for controlled filling of liquids into the channel, pump and valve structures (Lamberti, Marasso, and Cocuzza 2014). Here, in order to develop a centrifugable microfluidic chip, we used the vacuum connection, which allows the liquid to be filled into a closed flow channel with vacuum channels. Next, we demonstrated applications of density-based microparticle in a vacuum-integrated centrifugal microfluidic chip. The method includes filling characterization with vacuum integration into a straight channel. Then, microparticles with different densities were separated using density-gradient medium with 86% and 96.3% efficiency for 1.09 g/mL and 1.05 g/mL microparticles, respectively. This approach shows the air permeability property of PDMS has been simply applied to the centrifugal microfluidic chip system and it has been shown that it can be used for different separation approaches using the density-difference of cells.

2.2 Materials and Methods

Solidworks 2018 (Dassault Systemes, Canada) was used to design microfluidic structure, Preform (Formlabs, USA) was used as a 3D printer program and Formlabs Clear Resin (FLGPCL02, Formlabs, USA) was used for printing the molds. PDMS (Sylgard 184, Sigma-Aldrich, Germany) was used for the fabrication of microfluidic chip using soft lithography technique. Uncurable resin was removed by isopropanol (VWR International, U.S.A) and glass slides (Marienfield, Germany) were cleaned by ethanol (Merck, Germany).

To create microfluidic chip, spin coater (Spin Process Controller, Midas, Korea) and oxygen plasma (ZEPTO, Diener, Germany) were used. In order to make connection

between microfluidic chip and vacuum pump (5910100, Comecta Ivymen, Spain), needles (C3 Technology, Turkey) with 1.4 mm inner diameter and Tygon® tubing (Tygon® Saint-Gobain, U.S.A) were used. Ultimaker PLA 2.85 mm (Ultimaker, Netherlands) was used in the material of the tubes suitable for the centrifuge device (NF800R, Nüve, Turkey), and these tubes were produced with the Ultimaker 3D printer (Ultimaker Connect 2+, Ultimaker, Netherlands) device. In the study, microspheres (Cospheric LLC, CA) were used and prepared in Pluronic F-127(Sigma-Aldrich, Germany). Ficoll 400 solution (F4375-25G, Sigma-Aldrich, Germany) was used to create density-gradient layer. Microscope images were taken by Zeiss Axio Vert A1 inverted fluorescent microscope (ZEISS, Switzerland) with Colibri 7 Type RGB-UV LED illumination and Zeiss filter as FS 90 HE. Separated microparticles were analyzed by Python.

2.2.1. Experimental Setup

The fabrication of a microfluidic chip was performed using a soft lithography technique by printing the mold with UV curable resin. After printing, removal of resin residues was provided by washing the mold with isopropanol for 10 minutes. Elastomer and curing agent were mixed at a 10:1 ratio to prepare PDMS. Then, after the PDMS mixture was degassed and poured onto a mold, it was cured at 65 °C for 24 hours. Afterward, cured PDMS was peeled from the mold, clean glass was treated with oxygen plasma at 100 W and 0.5 mbar for 2 min. Then, PDMS was spun on clean glass by spin coater at 500 rpm for 10 s and 1000 rpm for 20 s and PDMS structure was bonded onto coated glass (Kecili and Tekin 2020).

Two different PDMS designs were used to achieve the characterization of sample loading and separation of microparticles according to their density differences. The first PDMS chip was designed with a fork-shaped vacuum channel and a fluidic channel (10 µl) with 1 mm (width) × 10 mm (length) × 1mm (height) dimensions (Figure 2.1. a) and distances between fluidic channels and control channels were determined as 1 mm (Figure 2.1. b). 10 µL food dye was used to calculate the rate of sample loading. The solution was given from the sample reservoir and the vacuum channel was connected with the vacuum pump using tubing. Time-dependent loading profile of food dye into a fluidic channel was investigated under a microscope.

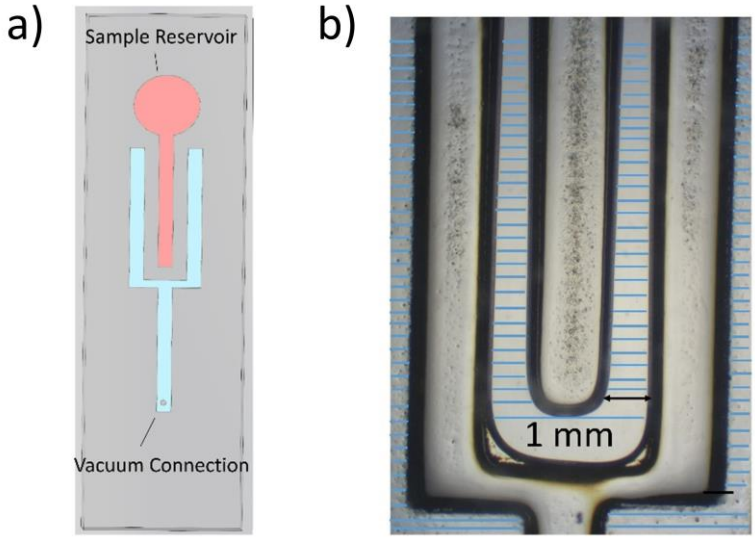

Figure 2.1. Vacuum-integrated fork-shaped microfluidic chip design. (a) Red channel and blue channel show a fluidic channel and vacuum channels, respectively. (b) Distance between the fluidic channel and vacuum channels designed as 1 mm; PDMS is shown as blue shaded regions. Scale bar is 200 μm. (Source: Oksuz and Tekin 2021)

For the density-based microparticle, second microfluidic chip was designed with a 500 μL volume each diamond shaped fluidic chambers consisted of 250 μL loading of the density-gradient media (Ficoll 400) and microparticles, respectively (Figure 2.2. a). The distance was adjusted to 1 mm between the fluidic channels and control channels (Figure 2.2. b).

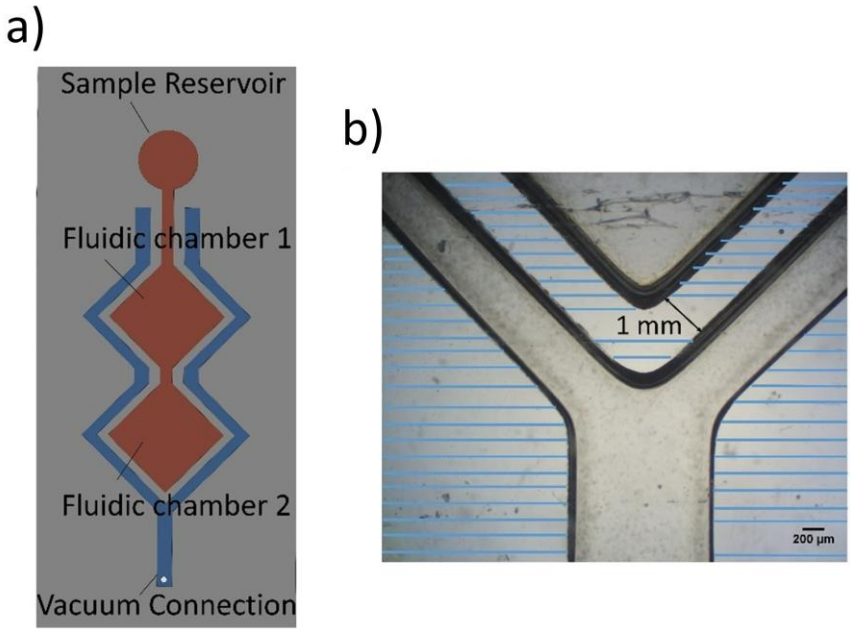

Figure 2.2. Vacuum-integrated diamond shape microfluidic chip design. (a) Red chambers and blue channels show a fluidic chambers and vacuum channels, respectively. (b) Distance between the fluidic chamber and vacuum channels designed as 1 mm; PDMS is shown as blue shaded regions. Scale bar is 200 µm. (Source: Oksuz and Tekin 2021)

2.2.2 Density-based Microparticle Separation

Separation of 1.02 g/mL-1.09 g/mL and 1.02 g/mL-1.05 g/mL microparticles were achieved by adjusting the density of Ficoll 400 as 1.065 g/mL and 1.035 g/mL, respectively. Afterward, 250 µLof Ficoll 400 was drawn from the sample chamber of the PDMS chip into the first diamond-shaped fluidic chamber by vacuum connection (Figure 2.3 (i)). Then, 250 µl microparticles prepared by Phosphate Buffered Saline (PBS) with 1% (w/v) Pluronic F-127 were given in the sample reservoir and withdrawn into the chip by vacuum connection. Then, to examine the separation efficiency of the microfluidic chip at 2000 rpm and 4000 rpm, the chip was placed in a centrifuge tube and centrifuged for different periods, and fluorescent images of the chip were obtained as a result of centrifugation.

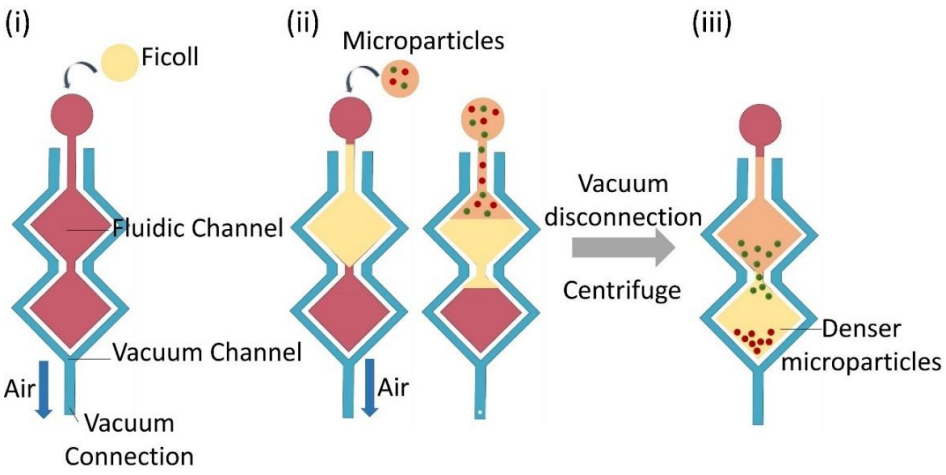

Figure 2.3. Microparticle separation protocol. (i) Ficoll and (ii) microparticle loading, and (iii) centrifugation

2.2.3 Statistical Analysis

All experiments were repeated three times unless stated, using a vacuum-integrated microfluidic chip. The data of a mean value of triplicates are shown in the graph as mean ± standard deviation (SD). The analyses were conducted by two-way analysis of variance (ANOVA) Tukey's multiple comparisons test using GraphPad Prism (version 8.0).

2.3 Results and Discussion

Here, a vacuum-integrated microfluidic chip was characterized using a straight fluidic channel and fork-shaped vacuum channel. Then, the separation efficiencies of microparticles having different densities were investigated in a diamond shaped vacuum-integrated microfluidic chip.

2.3.1 Characterization of Vacuum-Integration

In a fork-shaped PDMS chip, the loading of a red food dye solution through the fluidic channel took about 60 minutes with the vacuum connection from the vacuum

channels (Figure 2.4. a,b). On the other hand, to fill the fluidic channel of diamond-shaped PDMS chip, 140 min was necessary (Oksuz & Tekin, 2021).

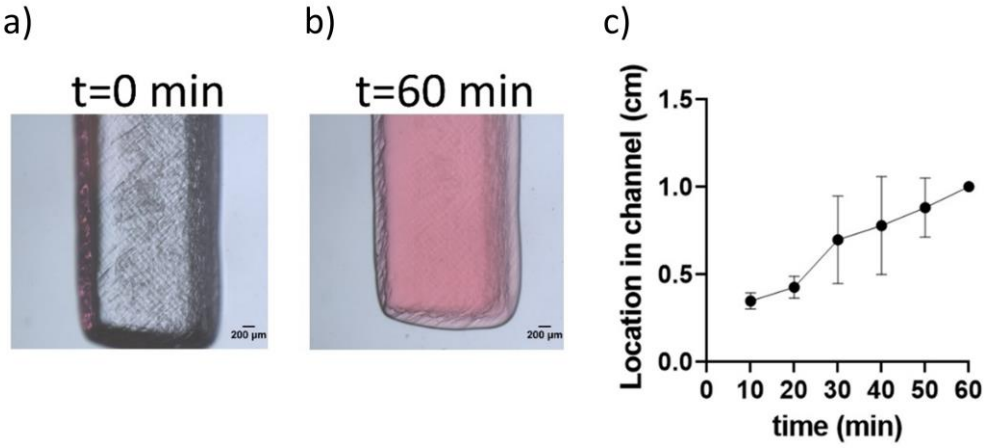

Figure 2.4. Time-dependent loading of food dye in a microfluidic channel. (a) Before vacuum is started and (b) after 60 minutes of vacuum (c) Position of food dye in a channel with different times of pumping. Scale bar is 200 µm. (Source: Oksuz & Tekin, 2021)

2.3.2 Density-based Microparticle Separation

We performed microparticles separation as density-based in a diamond-shaped PDMS chip and denser red fluorescent microparticles (1.09 g/m Land 1.05 g/mL) were sedimented at the end of the diamond-shaped chamber 2 separating from low-density (1.02 g/mL) green fluorescent microparticles. The microfluidic chip is assumed to be 100% across the two diamond shaped chambers, taking regions of the lower diamond chamber (0-15% and 0-30%) for high-density microparticles and taking regions (15-100% and 30-100%) for low-density microparticles (Figure 2.5.). Since the microparticles have different fluorescence, the separation efficiency was analyzed using Python code by counting the microparticles.

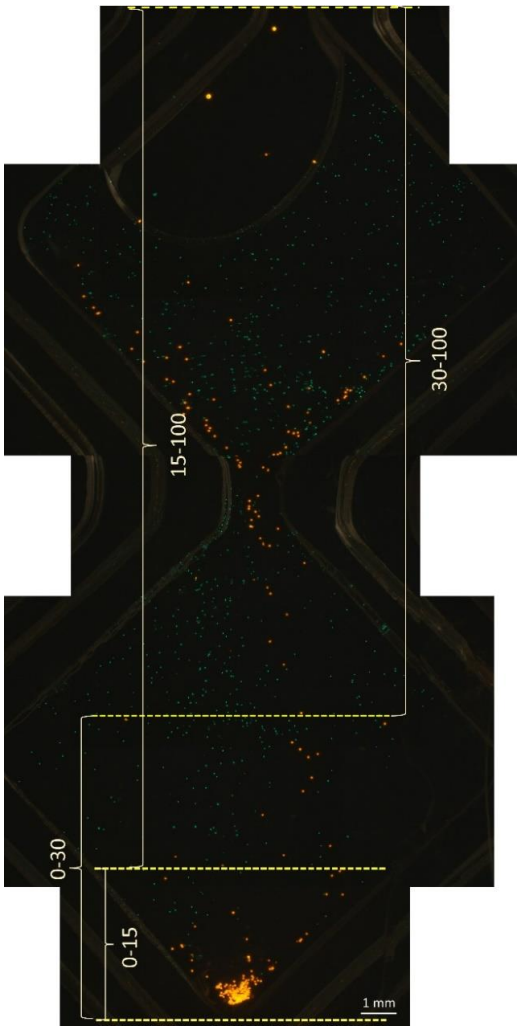

Figure 2.5. The separation zones as 0-15 and 0-30 for high-density microparticles, and as 15-100 and 30-100 for low-density microparticles.

According to our results, separation of 1.09 g/mL microparticles was achieved with 82.6% efficiency from 1.02 g/mL microparticles with 15 min centrifugation at 2000 rpm (Oksuz and Tekin 2021). The separation efficiency was slightly increased with increasing centrifugation time. However, a significant difference in separation efficiency and separation purity were not observed between different centrifugation time ($p < 0.05$).

At 4000 rpm, the highest separation efficiency of 1.09 g/mL microparticles was reached at 10th minutes (86%) at the 0-15 and 0-30 regions, while the separation of 1.02 g/mL was 13% in these regions (Figure 2.6. a). The separation of 1.02 g/mL microparticles in 15-100 region was observed as 97.6% at 8th minutes, by increasing the time it decreased to 96.7% (Figure 2.6. b). While there was no significant difference

between 0-15 and 0-30 regions in the separation of 1.09 g/mL microparticle, a significant difference was observed between 0-15 and 0-30 with other regions ($p < 0.05$). Likewise, while there was no significant difference between the 15-100 and 30-100 regions in the separation efficiency of 1.02 g/mL microparticles, a significant difference was observed between these regions and other regions ($p < 0.05$).

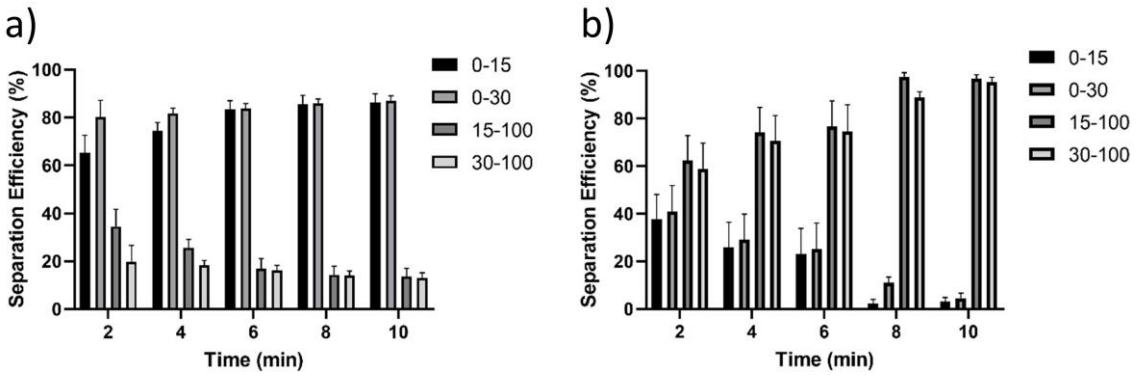

Figure 2.6. Time-dependent separation of microparticles with 1.02 g/mL and 1.09 g/mL at 4000 rpm. (a) Separation of 1.09 g/mL microparticles at different regions. (b) Separation of 1.02 g/mL microparticles at different regions

The separation of 1.02 and 1.05 g/mL microparticles with closer density to each other was investigated at different times at 2000 rpm and 4000 rpm (Figure 2.7. a). At 2000 rpm, the separation efficiency of 1.05 g/mL microparticles increased with increasing time and reached 86.7% in the 0-30 region at 30 minutes (Figure 2.8. a). However, while the separation efficiency of 1.02 g/mL microparticles was 93.7% at the 5th minute, it decreased to 87.79% in the 15-100 region at the 30th minute with increasing time (Figure 2.8. b). There was no significant difference between 0-15 and 0-30 regions in the separation of 1.05 g/mL microparticle, a significant difference was observed between 0-15 and 0-30 with other regions ($p < 0.05$). Likewise, there was no significant difference between the 15-100 and 30-100 regions in the separation efficiency of 1.02 g/mL microparticles, a significant difference was observed between these regions and other regions ($p < 0.05$).

At 4000 rpm (Figure 2.7. b), the separation efficiency of 1.05 g/mL microparticles increased with time and reached 96.3% in the 0-30 region at 8 minutes (Figure 2.8. c). Likewise, the separation efficiency of 1.02 g/mL microparticles in their region increased with time and reached 98.2% in the region of 15-100 at 8 minutes (Figure 2.8. d). There

was no significant difference between 0-15 and 0-30 regions in the separation of 1.05 g/mL microparticle, a significant difference was observed between 0-15 and 0-30 with other regions ($p < 0.05$). Besides, there was no significant difference between the 15-100 and 30-100 regions in the separation efficiency of 1.02 g/mL microparticles, a significant difference was observed between these regions and other regions ($p < 0.05$).

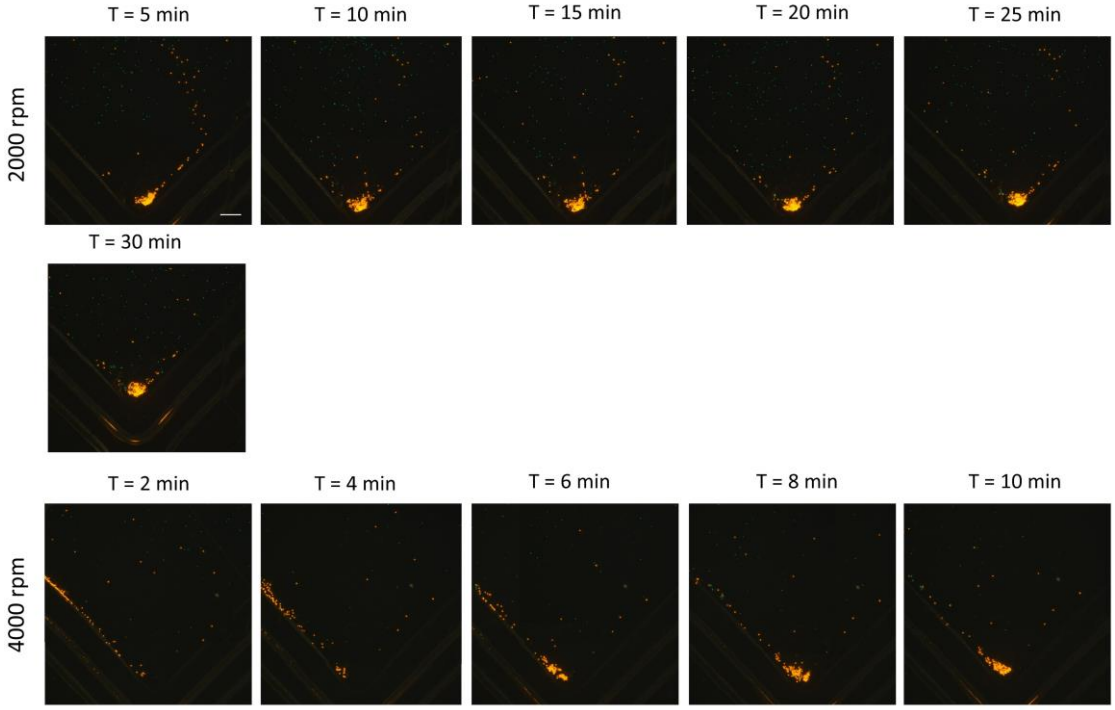

Figure 2.7. Time-dependent separation of 1.02 g/mL and 1.05 g/mL microparticles at 2000 rpm and 4000 rpm in 0-30 region. (a) Separation of 1.05 g/mL microparticles at 2000 rpm in 0-30 region. (b) Separation of 1.05 g/mL microparticles at 2000 rpm in 0-30 region

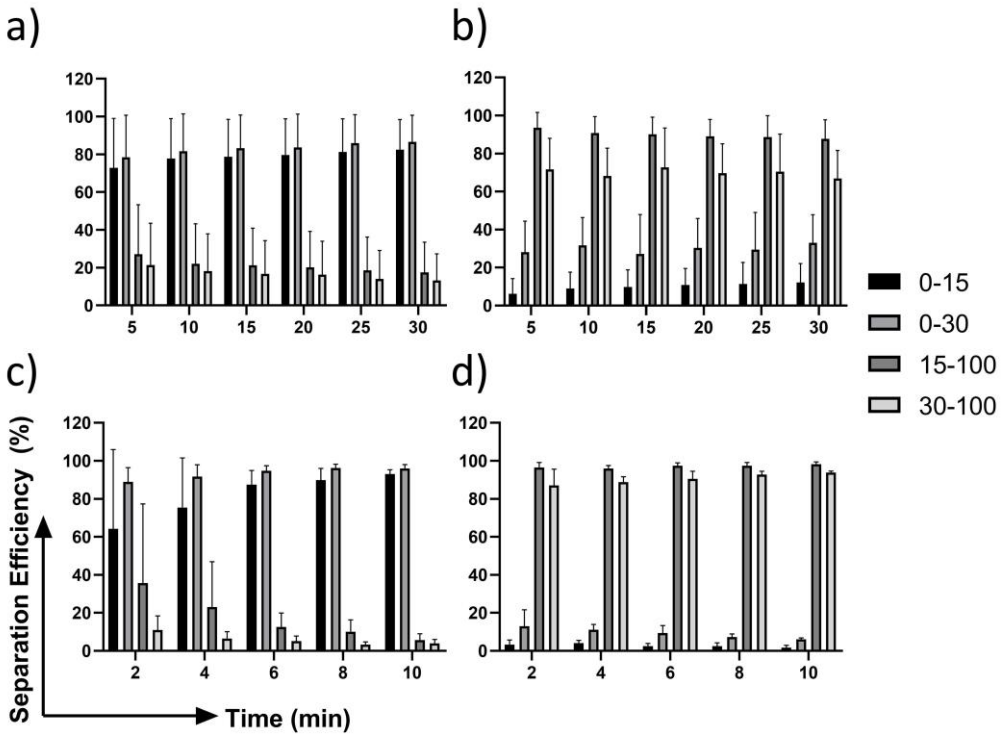

Figure 2.8. Time-dependent separation of 1.02 g/mL and 1.05 g/mL microparticles at 2000 rpm and 4000 rpm. (a) Separation of 1.05 g/mL microparticles applied 2000 rpm at different regions. (b) Separation of 1.02 g/mL microparticles at applied 2000 rpm at different regions (c) Separation of 1.05 g/mL microparticles applied 4000 rpm at different regions (d) Separation of 1.02 g/mL microparticles at applied 4000 rpm at different regions

2.4. Conclusions

In this study, we achieved density-based microparticle separation by combining the air permeability property of PDMS with a density-gradient solution with a different use. Thanks to the vacuum integration, the microfluidic chip was made suitable for the centrifuge by providing filling in the closed channel without opening the outlet. With this system, the cost of separation methods that require magnetic or fluorescent labels is eliminated, we have implemented it simply by adjusting the density-gradient medium, without using the membrane and valve structures in systems suitable for centrifugation. With this application, the separation of 1.09 g/mL microparticles from 1.02 g/mL microparticles reached 86% results in 10 minutes at 4000 rpm, while the separation of

1.05 g/mL microparticles from 1.02 g/mL microparticles at 4000 rpm reached 96.3% results in 8 minutes. Moreover, this low-cost operation of a system can be applied for cell separation by changing the density of a density-gradient medium and separated cells can be collected using a syringe thanks to the elastic structure of PDMS. The presented vacuum-integration principle can also be applied for a variety of cells such as blood components. This could enable the use of applications in the field of molecular and medical.

CHAPTER 3

SPINOCHIP: SPINNING AS A NOVEL TECHNIQUE FOR FLUIDIC MANIPULATION IN MICROFLUIDIC CHIPS WITH DEAD-END CHANNELS

3.1. Background

Since microfluidic systems mostly have inlet and outlet ports, it is not possible to apply the centrifuge principle in these systems. Active or passive valve structures are used to produce microfluidic chips suitable for the centrifuge system. In this chapter, for the first time in the literature, we have developed a centrifugal microfluidic approach that uses the inlet chamber as an outlet instead of using valve structures to allow filling into a closed channel. We explained the filling principle of the system developed using different channel sizes. Then, using this principle with multi-channel structures, we applied the sequential filling and metering properties of liquids. Finally, we used this developed approach in Chapter 4, for hematocrit measurement and WBC count, which are hematology tests frequently applied in hospitals. Thanks to this approach, it has been proven for the first time that fluid manipulations can be performed from the same inlet and outlet in a closed channel, and that this system can be used successfully in clinical tests as well as for applications such as molecular separation and enrichment.

3.2 Materials and Methods

Solidworks 2018 (Dassault Systemes, Canada) was used to design 2D microfluidic channels and reservoirs. Designed channels and reservoirs were cut by laser cutter (Laserbox Pro, Makeblock, China) using optically clear adhesive having 0.75 mm thickness (Thorlabs, USA) and polymethyl methacrylate (PMMA) (Depodanmalzeme, Turkey), respectively. Bonding of layers were completed onto the glass slides (Marienfield, Germany).

Characterization of microfluidics were performed by spin coater (Spin Process Controller, Midas, Korea) using a spinning platform consist of cassettes for microfluidic chip and Xiaomi Redmi Note 8 Pro (Xiaomi, China) and Iphone 6S (Apple, USA) smartphones made by Ultimaker PLA 2.85 mm (Ultimaker, Netherlands) and printed by Ultimaker (Ultimaker Connect 2+, Ultimaker, Netherlands). Food dye (Deembro, Turkey) with different colors was used for the observation of fluid profile and it was analyzed by Adobe Photoshop 2021 (Adobe Inc., USA).

3.2.1 Experimental Setup

To demonstrate the fluid manipulation and characterization of the system, a platform compatible with the spin coater device, with the same rotor distance as the centrifuge device used in Chapter 4, was designed. The platform includes two sockets 104 mm from the center (r) and at an angle of 45º with the platform, which is used to accommodate the chips,and a socket to place the smartphone in the middle (Figure 3.1. a). Microfluidic chips were fabricated using 1 mm clean glass at the bottom, 2 mm PMMA layer contains reservoirs at top and fluidic channels in the middle with DSA film each layer has 75 μm thickness. The forces applied to the channel during rotation are centrifugal force (Fcnet), Coriolis force (Fcor) and capillary force (Fcap) depending on the rotation speed (Figure 3.1. b).

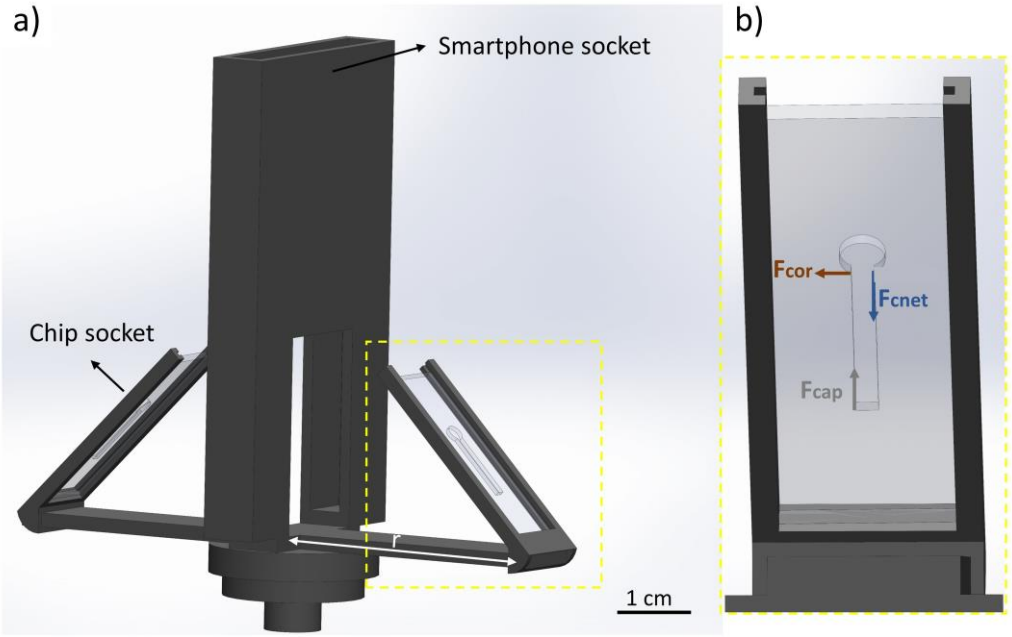

Figure 3.1. The spinning platform suitable for spin coater device. (a) Components of a spinning platform. (b) Forces applied to a channel while spinning

3.2.2 Characterization of Spinochip

Straight channels using different channel widths (1-4 mm), different channel heights (75-225 um) and different channel lengths (12.5-37.5 mm) were designed to explain the principle and filling profile that enables filling into the closed channel (Figure 3.2.). By using 20-30 µl of food coloring for each channel, the rotational speeds depending on the channel properties were determined, and the relationship between the rotational speed required for filling of each channel and the hydraulic resistance (Equation 3.1) was specified:

$$R = \frac{1}{1-0{,}63\,(\frac{h}{w})}\,\frac{12\,\mu L}{h^3 w} \qquad (3.1)$$

,where h is the height of a channel, w is the width of a channel, L is the length of a channel and µ is the dynamic viscosity.

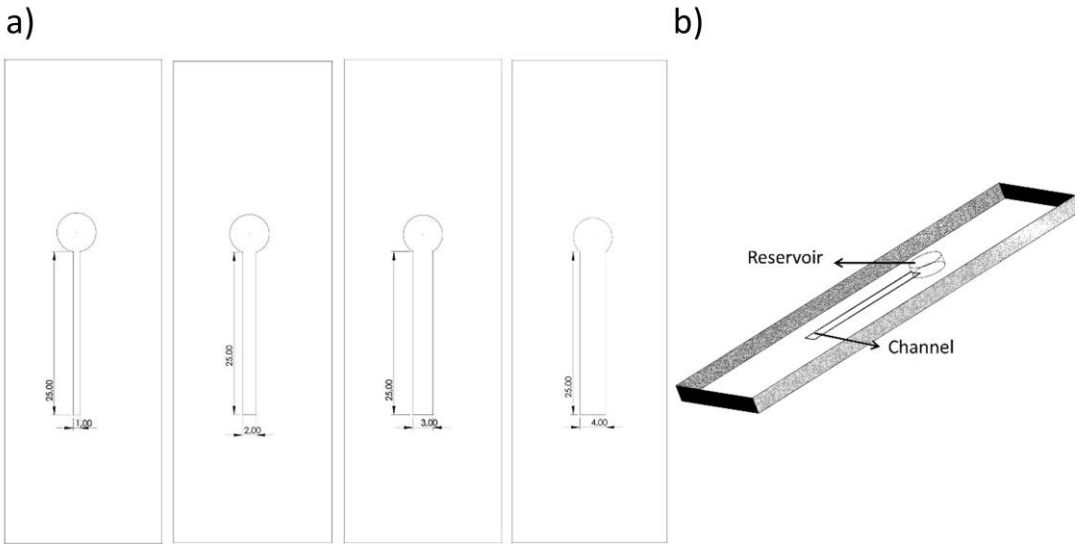

Figure 3.2. Illustration of a channel design. (a) Straight channels with different widths (b) A channel consists of one straight channel and one reservoir connected with closed channel.

By keeping the rotation speed constant, the video of each channel was framed in one tenth of a second during the rotation, and the time-dependent filling profile was examined in the Adobe Photoshop program and the relationship between the time required for filling and the hydraulic resistance was given.

3.2.3. Sequential Filling in Spinochip

Three channels with channel widths of 4 mm, 2 mm, and 1 mm and a reservoir layer with 150 μm height connected to each channel were created with DSA to demonstrate sequential filling on the chip. Holes with a diameter of 1 mm were formed on 1 mm PMMA to fill the liquids in the upper layer into the lower chamber. The sequential filling principle was demonstrated on two different chips; first design where three channels were connected to a straight channel and a collection chamber of 16 μL volume (Figure 3.3. a), the second design where three channels were connected to the collection chamber of 16 μL volume via a junction (Figure 3.3. b). For sequential filling, 5 μl of different colors of food dye were filled with a pipette into each reservoir by holding the chip upside down. Then, by applying the rotational speeds obtained in chapter 3.2.2 according to the channel width and height used, the liquids were released at their rotation speed from their chambers in order. The results were both photographed and recorded.

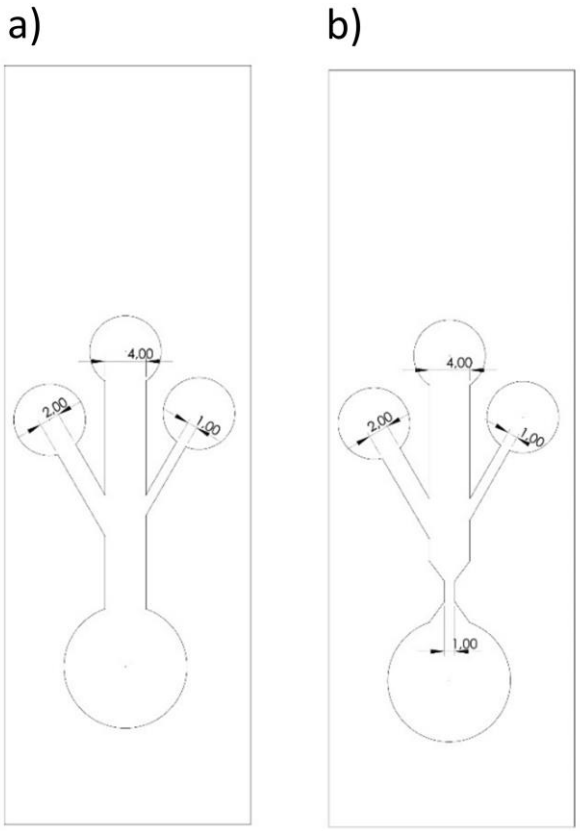

Figure 3.3. Illustration of a sequential filling channels. (a) Straight channels connected with the collection chamber. (b) Straight channels connected with the collection chamber via a junction.

3.2.4 Statistical Analysis

Unless stated, all experimentes were performed as triplicates using a Spinochip for each experiment. The data of mean value of triplicates are shown in the graph as mean ± standard deviation (SD). The analyses were conducted by two-way analysis of variance (ANOVA) Tukey's multiple comparisons test using GraphPad Prism (version 8.0). Standard equations for rotation speeds and the hydraulic resistance were obtained from the fitted linear curves (semilog lines) of experimental data.

3.3. Results and Discussion

Here, for the first time in the literature, the filling principle of the closed microfluidic channel, which provides the inlet and outlet from the same place, was characterized by different channel properties. Fluid manipulation was demonstrated on a chip that provides sequential filling with diode characteristics with hydraulic resistance varying according to channel size. The same principle has been implemented with cassettes with 0º, 45º, 60º and 90º angles on the platform. As a result, it was observed that the liquid did not fill into the channel in cassettes with an angle of 60º and 90º degrees.

3.3.1 Principle of SpinoChip

Demonstration of filling principle of Spinochip was performed by using variety of channel properties such as width (1-4 mm) and height (75-250 μm). Each channel was tested on the spin coater platform, starting at 100 rpm for 5 minutes, until the channel was filled. It was concluded that different rotational speeds were required for filling at each channel width and height (Figure 3.4.) According to our results, increament in channel width and channel height decreases the rotation speed require fluid to be filled in the channel.

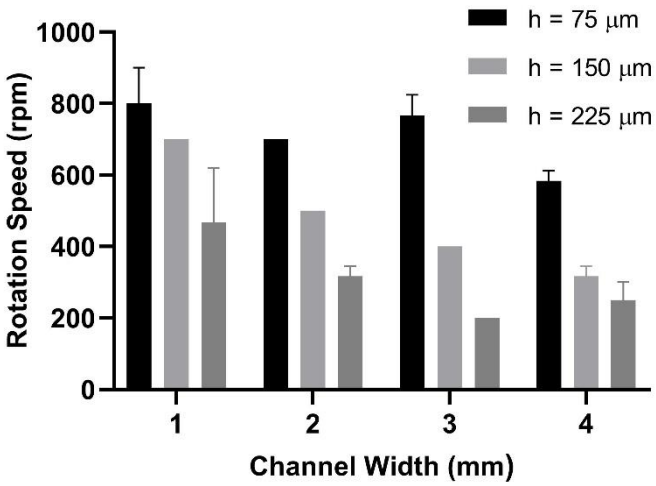

Figure 3.4. Rotation speed required for a channel to be filled varying with width and height of a channel.

It was observed that the liquid first formed a meniscus structure at the entrance of the channel, and then, with the advancement of the liquid, it pushed the air in the channel into the reservoir and fills into the channel with the centrifugal force (Figure 3.5.).

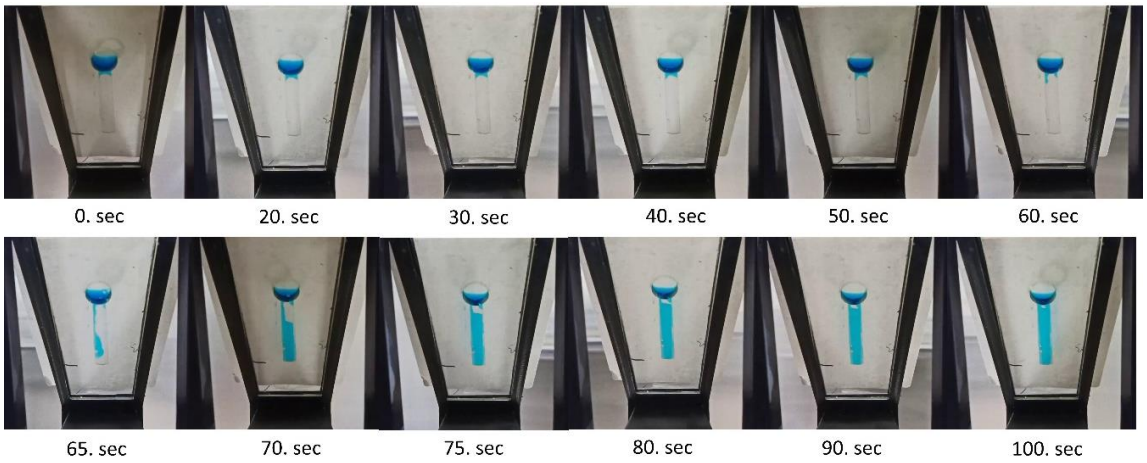

Figure 3.5. A closed channel filling with the centrifugal force by pushing the air to a reservoir

3.3.2. Characterization of Spinochip

The hydraulic resistance depending on the channel size changes and the principle of Spinochip was revealed with it (Figure 3.6.). Hydraulic resistance increases with decreasing the channel height and width. According to our results, there is a linear corelation between hydraulic resistance and rotation speed for the channel to be filled. This proves that the different channel sizes on the same microfluidic chip can be programmed for different rotation speeds and different flow profiles.

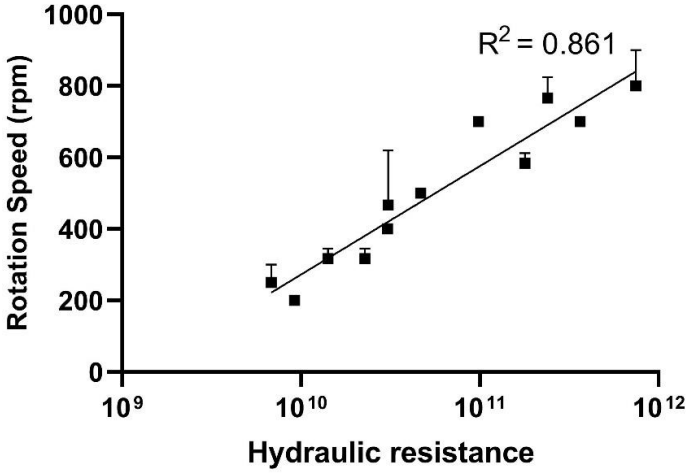

Figure 3.6. The relation between hydraulic resistance of different channel sizes and rotation speeds where channel is completely filled

For the characterization of the Spinochip filling, the filling of channels with different lengths were investigated by keeping the channel width and height constant. With this regard, 2 mm channel width, 150 μm channel height and different channel lengths (12.5 mm, 25 mm and 37.5 mm) exposed to same rotation speed (500 rpm) to see the filling behavior in a channel. According to our results, it was clearly seen that shorter channels filled faster than the longer channels (Figure 3.7.). Also, it was observed that in shorter channels, the meniscus structure formation, pushing the air inside the channel into the reservoir were faster and thus filling of liquid inside a channel was faster.

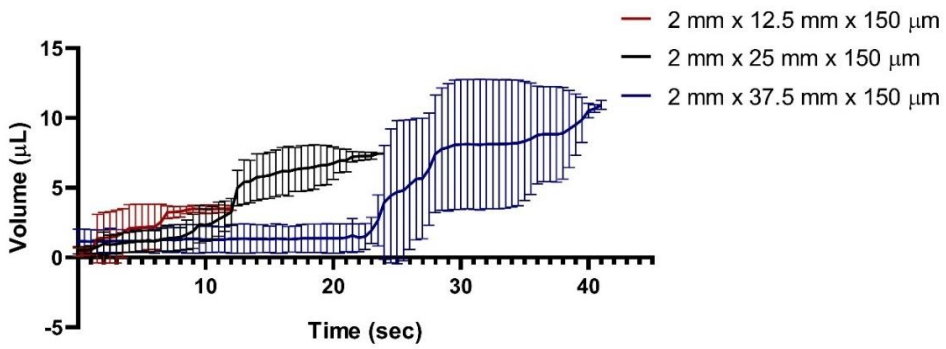

Figure 3.7. The volume profile of channels with different lengths and same width and height.

Filling behavior in a channel depend on the channel width and length was explained related with the hydraulic resistance. With this regard, to observe the flow profile of channels with 2 mm, 3 mm and 4 mm widths and 25 mm lengths were exposed to the same rotation speed (500 rpm). According to our results, in wider channels, the meniscus structure formation, pushing the air inside the channel into the reservoir were faster and thus filling of liquid inside a channel was faster (Figure 3.8.).

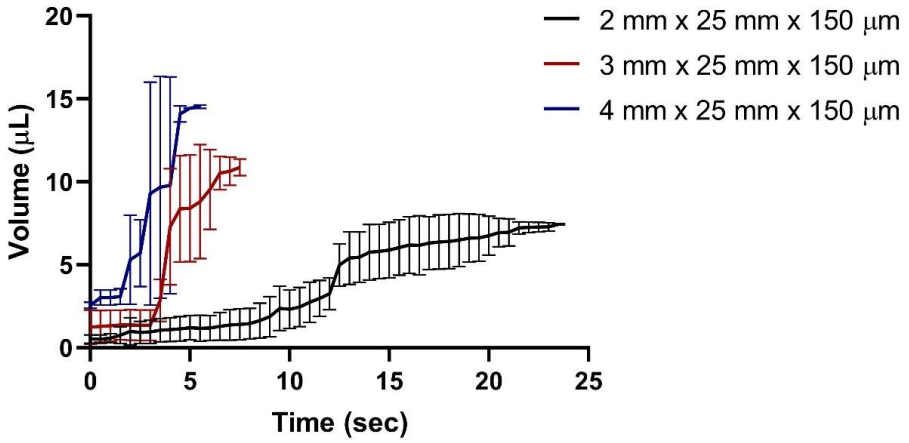

Figure 3.8. The volume profile of channels with same length and same height with different widths.

We have shown how the filling profile is related to keeping the force constant across different channel widths and lengths. In this context, we revealed that the

relationship between the filling speed of the channels by calculating the hydraulic resistances according to the lengths and widths of the channels used (Figure 3.9.). According to our results, there is a linear corelation between hydraulic resistance and filling time of a channel under the same rotation speed. This proves that the wider and shorter channels filled faster.

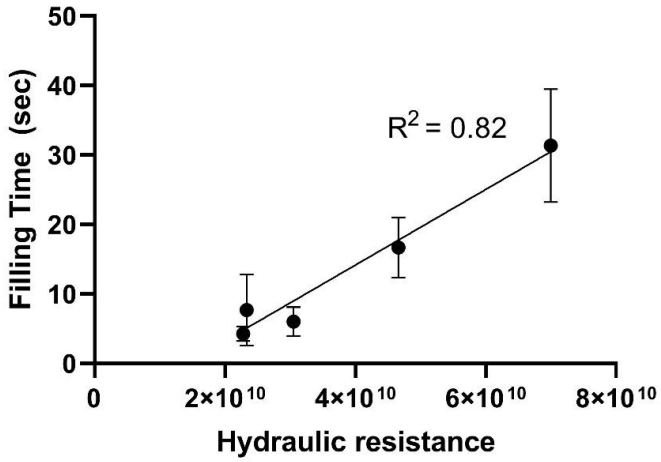

Figure 3.9. The relation between the filling time of channels and hydraulic resistance

3.3.3. Sequential Filling in Spinochip

In Chapter 3.3.1, the diode property was shown with the required rotation speed determined to fill each channel, and this property was applied to the sequential filling principle of the Spinochip (Figure 3.10.). Holding the chip upside down, 4 µl of food dye from each hole was given with a pipette, red to the reservoir with 4 mm channel, blue to the reservoir with 2 mm channel, and green to the reservoir with 1 mm channel. Then, the chip was rotated on the rotation platform placed on the spin coater. At 300 rpm for 5 seconds, 500 rpm for 10 seconds, and 700 rpm for 10 seconds to release the liquids in the reservoirs connected to the 4 mm, 2 mm and 1 mm channels, respectively.

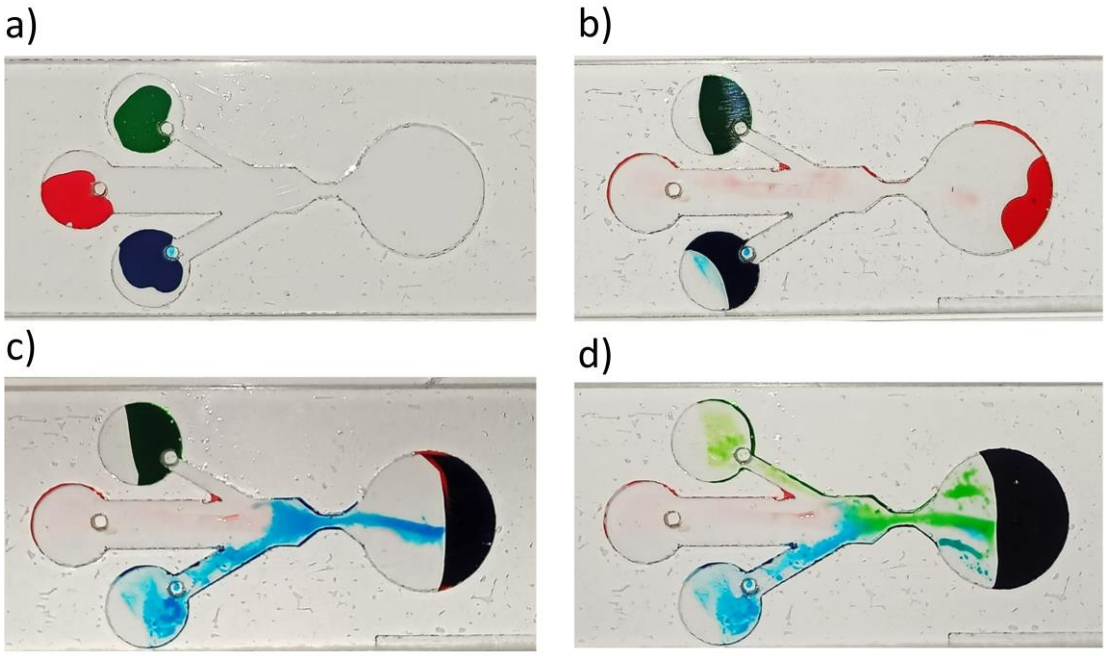

Figure 3.10. Sequential filling of Spinochip. (a) Food dye was injected to each reservoir from the top hole. (b) Liquid from the reservoir connected to the 4 mm channel was released applying a 300 rpm. (c) Liquid from the reservoir connected to the 2 mm channel was released applying a 500 rpm. (d) Liquid from the reservoir connected to the 1 mm channel was released applying a 700 rpm.

3.4. Conclusions

In this study, we achieved for the first-time filling of a closed channel using the same reservoir as an inlet and an outlet applying the centrifugal force. Microfluidic chips require inlet and outlet holes until now. On the other hand, passive and active structures were needed for microfluidic chips in accordance with the centrifuge principle to work in a closed channel. Thanks to the Spinochip, a closed-channel microfluidic chip can, for the first time, provide filling into the channel without the use of additional structures, acting as an inlet and outlet from a single reservoir, at low-cost. In order to explain the filling principle, we determined the rotation speeds required to fill the channels using different channel widths and heights. We proved that the system can provide a diode property by showing the relationship of these rotational speeds with hydraulic resistance. Then, we examined the filling profile with different channel parameters and the hydraulic

resistance and filling speed of these channels. As a result, we found that wide, long and high channels push the air faster, thus liquid filled faster into the channel. Finally, we demonstrated a sequential filling within the microfluidic chip, where channels of different widths were connected to a collection chamber. This novel and low-cost operation of a system can be utilized for clinical tests, molecular studies, cell separation, enrichment and purification. It can be automated and made suitable for assays by applying different fluid manipulations on the system. At the same time, it can lead to point-of-care studies by developing it into a device.

CHAPTER 4

BLOOD SAMPLE MANIPULATIONS IN SPINOCHIP

4.1. Background

Many diseases can be diagnosed, or their treatment method can be determined by separating the cells in the blood sample. However, the methods and devices applied in the clinic are quite bulky and expensive, and they also require technicians, consume high volume of reagents and samples. Here, we use 10 μL of whole blood sample for plasma separation to measure the hematocrit value and to estimate WBC number from buffy coat region in a single channel with the Spinochip. Then, we compared the hematocrit and WBC results obtained from Spinochip with the patient results in the clinic. First, we achieve the plasma separation from whole blood and we obtained three layers as red blood cells, buffy coat and the plasma. Then we measure the hematocrit value from the ratio of the volume occupied by the RBCs to the total volume. Then, we perform WBC estimation from the buffy coat region by measuring the thickness of a buffy coat. System enables hematocrit measurement and WBC count in a less time (10 min) with a low amount of sample volume (10 μL).

4.2. Materials and Methods

Solidworks 2018 (Dassault Systemes, Canada) was used to design 2D microfluidic channels and reservoirs. Designed channels were cut by laser cutter (Laserbox Pro, Makeblock, China) using optically clear adhesive having 0.75 mm thickness (Thorlabs, USA) and reservoirs were cut by laser cutter (Laserbox Pro, Makeblock, China) and used polymethyl methacrylate (PMMA) (Depodanmalzeme, Turkey). Bonding of layers were completed onto the glass slides (Marienfield, Germany). Ultimaker PLA 2.85 mm (Ultimaker, Netherlands) was used as the material of the tubes suitable for the centrifuge device (NF800R, Nüve, Turkey), and these tubes were produced with the Ultimaker 3D printer (Ultimaker Connect 2+, Ultimaker, Netherlands).

Blood samples taken from Dr. Suat Seren Chest Diseases Hospital approved by the ethics committee decision numbered 11.05.2022/26-33 were stained by Hoescht 33342 (Thermo Fisher Scientific, USA) and the blood sample in the Spinochip was placed in a centrifuge device (NF800R, Nüve, Turkey). Microscope images were taken by Zeiss Axio Vert A1 inverted fluorescent microscope (ZEISS, Switzerland) and images were taken by Xiaomi Redmi Note 8 Pro (Xiaomi, China). Results were analyzed using ImageJ (National Institutes of Health, USA) and Adobe Photoshop 2021 (Adobe Inc., USA).

4.2.1. Experimental Setup

As specified in Chapter 3, a straight channel with a volume of 10 μL was used for the separation of whole blood samples in Spinochip with the centrifugation (Figure 4.1. a). A PLA tube was designed and formed in order for the Spinochip work stable in the centrifuge device (Figure 4.1. b).

Figure 4.1. The design of Spinochip for blood sample manipulation. (a) A straight channel with a 23 mm length, 3 mm width and 0.15 mm height. (b) A tube suitable for the centrifuge device for the Spinochip

4.2.2. Plasma Separation

Different rotation speeds and times were examined to ensure plasma separation of 10 µl whole blood sample in Spinochip. Then, by looking at the number of cells remaining in the plasma, the rotation speed and time with the minimum cell number were used to determine the hematocrit values. The hematocrit value was determined by measuring the volume of RBC in the Spinochip and the total volume using the ImageJ program (Equation 4.1).

$$\%\text{Hct} = \frac{\text{Volume of RBC}}{\text{Total volume in a microfluidic}} \times 100 \quad (4.1)$$

4.2.3. White Blood Cell Estimation

Hoescht fluorescent dye was added at a ratio of 1:1000 (v/v) to the whole blood sample taken in an EDTA tube and incubated at 37°C for 15 minutes. The whole blood sample was diluted 1:2, 1:4, and 1:6 (v/v) with PBS to create the calibration curve for WBC estimation. Spinochip was placed in the centrifuge device in the PLA tube and centrifuged at the rotation speed and time determined in Chapter 4.2.2. After the centrifugation, buffy coat images were taken. The thickness of the formed buffy coat region was examined and their correlation with the WBC count. Then, 6 patient samples taken into the EDTA tube were stained with Hoescht and 10 µl was put into the chip. The buffy coat thickness was measured with the ImageJ program by centrifuging at the rotational speed and time specified in Chapter 4.2.2, and the results were compared with the patient results in the clinic.

4.2.4. Collection of A Plasma Sample

In order to collect the separated plasma of whole blood samples that have achieved plasma separation, a 10 µL volume chip was designed with two channels, one of which has a hole to collect the sample (Figure 4.2.). Plasma sample was collected from the chip of blood samples whose plasma separation was achieved.

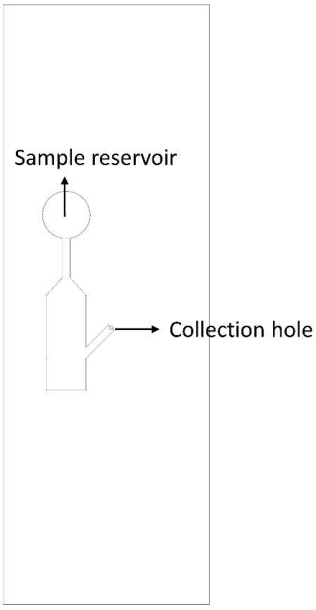

Figure 4.2. Two-channel plasma collection microfluidic chip with a sample reservoir and a collection hole.

4.2.5. Sample Selection for Clinical Tests

For the study, blood samples taken from patients or healthy individuals who applied to Dr. Suat Seren Chest Diseases and Chest Surgery Training and Research Hospital and sent for hemogram in the Medical Microbiology Laboratory were studied. As a result of the hemogram analysis, the sample within the range of 30-60% for hematocrit measurement and 4-11 $x10^3$ /μL for white blood cell count was used.

4.2.6. Statistical Analysis

All blood experiments were performed as triplicates unless stated, using a Spinochip for each experiment. The data of mean value of triplicates are shown in the graph as mean ± standard deviation (SD). The statistical analyses were conducted by two-way analysis of variance (ANOVA) Tukey's multiple comparisons test using GraphPad Prism (version 8.0). The correlation between the results were computed using two-tailed GraphPad Pearson correlation test.

4.3. Results and Discussion

Here, dead-end Spinochip was applied for routine clinical tests hematocrit measurement and WBC counting. For the first time in the literature, a buffy coat region was observed in the channel which provides an information about platelets and WBCs. Plasma was separated in a channel and hematocrit measurement provided. Then, WBC estimation was made from buffy coat region as thickness of buffy coat and fluorescence intensity in that region. Besides, two-channel centrifugal microfluidic chip was used to collect separated plasma sample. As a result, hematocrit (%) results and WBC numbers obtained from the Spinochip were significantly correlated with the clinical results.

4.3.1. Plasma Separation

Plasma separation from 10 μL of whole blood was examined applying different rotation speeds (Figure 4.3. a). According to our results, it was clearly seen that there was no significant change in plasma volume depend on the rotation speed and time ($p < 0.05$). Plasma color was controlled with the Hemolysis Reference Palette (CDC 2021) after the blood samples were centrifuged in the chip at different rotation speeds and no hemolysis was observed (Figure 4.3. b).

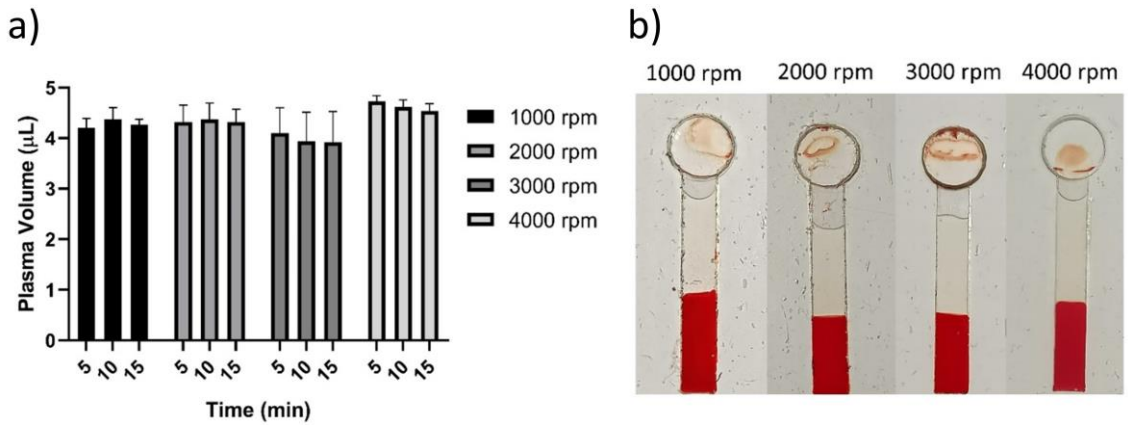

Figure 4.3. Plasma separation from whole blood sample. (a) The change of a plasma volume with respect to rotation speed and time (min). (b) Plasma separation images at different rotation speeds.

Determination of rotation speed and time required for a plasma separation was made by counting the cells stayed in a plasma region. At 1000 rpm and 2000 rpm, cells were much more than 3000 rpm and 4000 rpm in plasma region (Figure 4.4.). At 4000 rpm, number of cells in a plasma was decreasing with the time and there was no difference between 10 minutes and 15 minutes. Thus, 4000 rpm 10 minutes was selected for a plasma separation and hematocrit measurement.

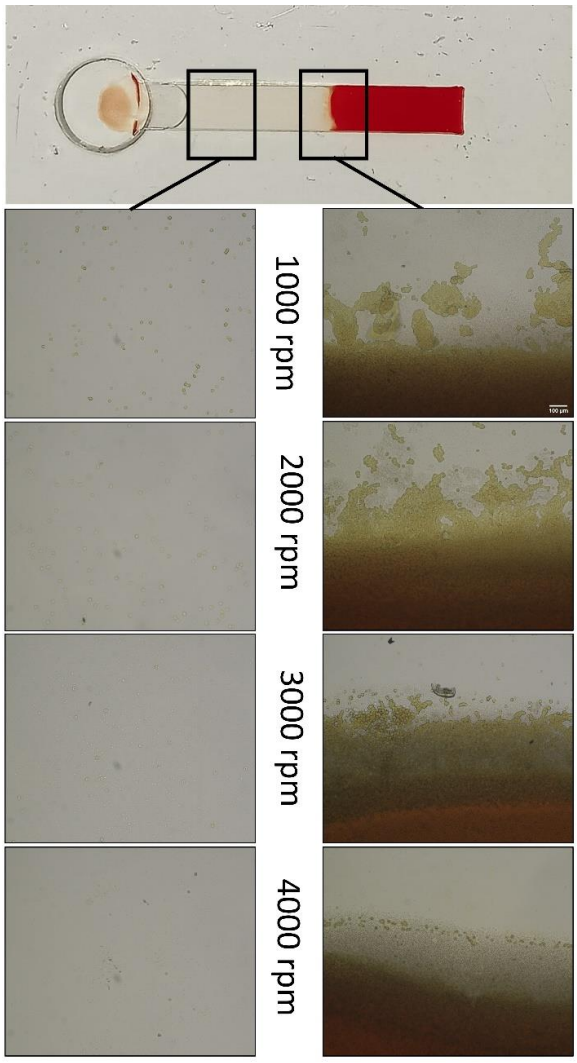

Figure 4.4. Plasma separation from whole blood sample at different rotation speeds for 10 minutes in a Spinochip. Left: Cells in a plasma region Right: Buffy coat formation. Scale bar is 200 μm.

Centrifugation of a Spinochip filled with whole blood created a middle layer between plasma and RBC region (Figure 4.5. a). Normally, this layer would be buffy coat

region and consists of WBCs and platelets. To verify this, whole blood was stained with Hoescht fluorescent dye and observed under a microscope (Figure 4.5. b,c). It was proved that the layer consisted of WBCs and this region could not be observed using 1 mL of whole blood in an Eppendorf by centrifugation.

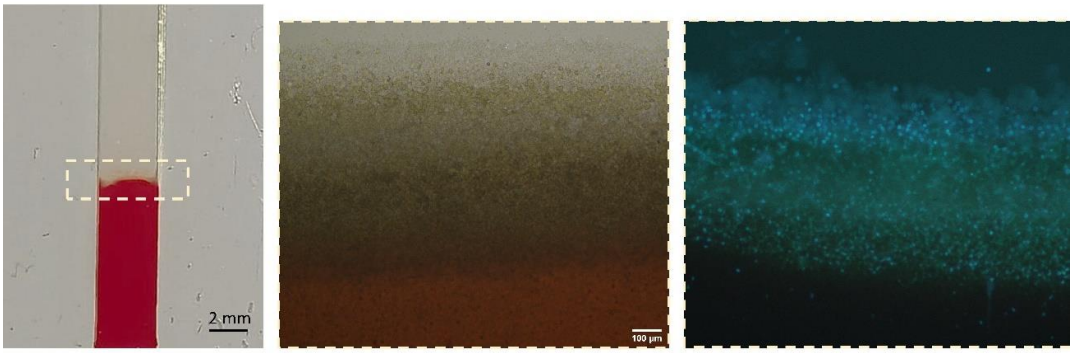

Figure 4.5. Buffy coat formation from whole blood sample. (a) Buffy coat region observed with the smartphone camera. (b) Bright-field image of a buffy coat region. Scale bar is 100 µm. (c) Fluorescent image of a buffy coat region shows the WBC.

4.3.2. Hematocrit Value Measurement

Hematocrit value (%) was measured using Equation 4.1. Hematocrit results taken from Spinochip were compared with clinical patient results (Figure 4.6.). According to our results, there is a significant correlation between the measurements taken in the Spinochip and the clinical results.

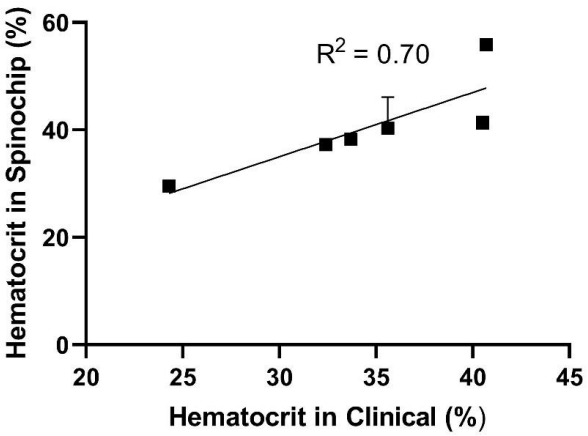

Figure 4.6. The comparison of a hematocrit measurement in Spinochip and clinical results.

4.3.3 White Blood Cell Estimation

Whole blood stained with Hoescht fluorescent dye was diluted with PBS at 1:2, 1:4, 1:6 ratios and centrifuged at 4000 rpm for 10 minutes in the chip, and the buffy coat region was examined. When looking at the microscope images, it was seen that the buffy coat thickness decreases with the dilution (Figure 4.7.).

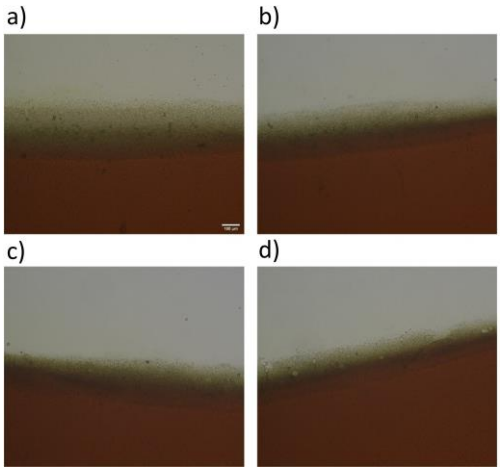

Figure 4.7. Microscope images of buffy coat region. (a) Buffy coat region of whole blood sample. (b) Buffy coat region of 1:2 diluted blood. (c) Buffy coat region of 1:4 diluted blood. (d) Buffy coat region of 1:6 diluted blood.

In order to measure the thickness of the buffy coat region for WBC estimation, brightfield images were verified with fluorescent images, and measurements were taken with ImageJ program from 6 equidistants of a buffy coat (Figure 4.8.).

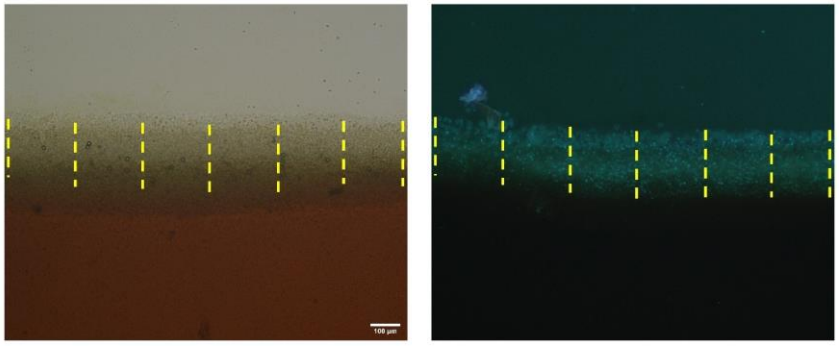

Figure 4.8. The measurement of a buffy coat thickness. (a) Brightfield microscope image of a buffy coat region was separated 6 equidistant pieces. (b) Fluorescent microscope image of a buffy coat region was separated 6 equidistant pieces.

A calibration curve was created with the measurement of buffy coat thickness in order to make WBC estimation from the blood sample, whose WBC was concentrated by precipitation of whole blood in eppendorf and removing the plasma, also whole blood diluted at different ratios. According to our results, there is a significant correlation between the buffy coat thickness and WBC numbers in a blood (Figure 4.9.).

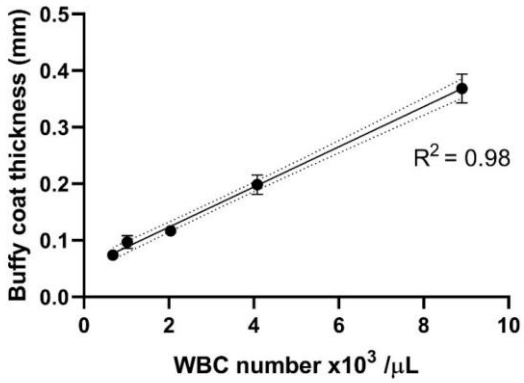

Figure 4.9. The correlation between the buffy coat thickness and the WBC number in a blood sample.

Using the equation obtained from the calibration curve in Figure 4.9, the measured buffy coat thickness of the patients was substituted in this equation and the corresponding WBC number was obtained. According to the results, there is a significant correlation between the WBC counts obtained in the clinic and Spinochip (Figure 4.10).

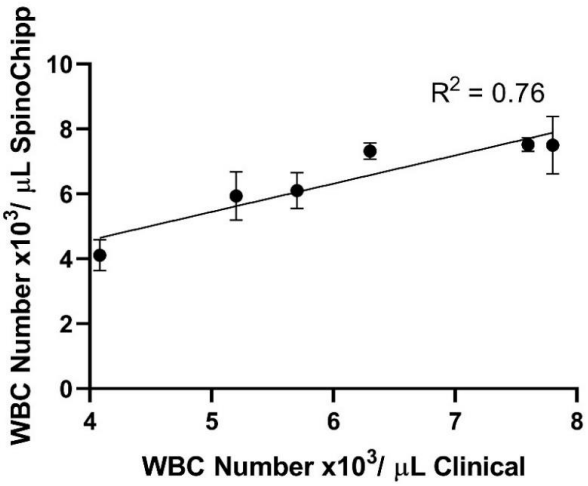

Figure 4.10. The correlation between the buffy coat thickness and the WBC number in clinical results.

4.3.4. Collection of A Plasma Sample

10 µl of whole blood sample was centrifuged at 4000 rpm for 10 minutes in a two-channel microfluidic chip and buffy coat formation was observed in the chip. Then, the separated plasma sample was collected with a pipette from the collection hole and examined under the microscope. As a result, it was observed that there were no cells in the collected plasma, but some of the plasma sample remained in the chip. In addition, it was seen that the buffy coat region was not damaged as a result of collecting the plasma sample from the chip with a pipette (Figure 4.11).

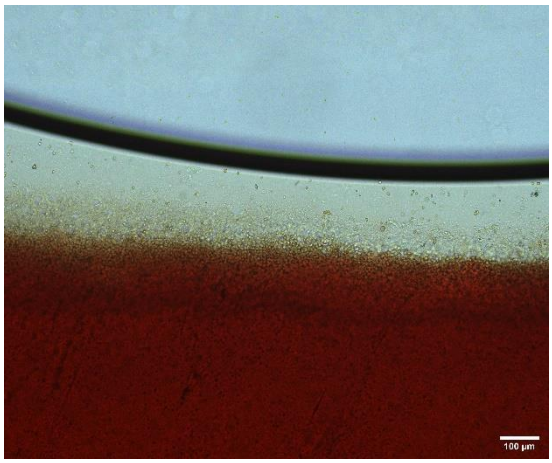

Figure 4.11. A buffy coat region after the separated plasma was collected from the chip.

4.4. Conclusions

In this study, we applied hematocrit measurement and WBC count which are one of the routine clinical blood tests, on the Spinochip in the same channel. Clinical methods and devices are quite bulky and expensive, and they also require technicians, consume high volume of reagents and samples. Moreover, buffy coat formation by plasma separation from whole blood and WBC estimation depending on buffy coat thickness was performed for the first time in the microfluidic chip. In this context, the rotation speed and time required for plasma separation from the whole blood sample were determined, and the hematocrit value was calculated and a significant correlation was found with the results obtained in the clinic. Next, a calibration curve was created by correlating the buffy coat thickness and the WBC count from the precipitated and diluted whole blood sample. By replacing the measured buffy coat thickness of the patients in the equation obtained here, a significant correlation was found between the number of WBCs measured in the chip and clinical results. Thus, it was shown that Spinochip can be applied in clinical testing. It is also presented that many different clinical tests can be performed on a single chip by increasing the number of channels on a single chip. By changing the chip structure with PDMS, the cells separated in the chip can be collected more precisely.

CHAPTER 5

NEGATIVE MAGNETOPHORESIS MICROFLUIDIC CHIP

5.1. Background

Separation techniques that require labeling necessiate labor-intensive sample handling and expensive equipment. Separation of cells according to their size and deformability is achieved by microfilter structures. However, the high cost of microfabrication and the problem of clogging in physical structures limit the utilization. Methods that provide size-dependent cell/microparticle separation in determined lateral displacement, inertial separation, compressed flow separation, and acoustic separation also have disadvantages such as particle loss, particle-particle interaction, inefficient separation. Here, we developed a negative magnetophoresis technique in a microfluidic chip can separate microparticles and cells using their size differences. Thus, we have eliminated the need for labeling methods, expensive solutions and complex methods. Microparticles/cells added to the paramagnetic environment can differ according to their size difference in the microfluidic channel where placed between two magnets. Large microparticles/cells are captured by negative magnetophoresis, while small ones pass through the magnets. System enables capturing of 25 μm microparticles from 15 μm microparticles with > 98.5% at 6.5 μL/min flow rate and removing of U937 cells from the magnets with 95.47% at 9 μL/min flow rate, while an 89.6% of MCF-7 cells were captured between magnets.

5.2. Materials and Methods

Solidworks 2018 (Dassault Systemes, Canada) and AutoCAD (Student Version, Autodesk Inventor, California) were used to design 2D microfluidic channels and magnet rings for Nedoymium magnets (K&J Magnetics Inc., USA). Designed channels and magnet holders were cut by laser cutter (Laserbox Pro, Makeblock, China) using double-side adhesive having 0.75 mm thickness (Thorlabs, USA) and PMMA

(Depodanmalzeme, Turkey), respectively. Bonding of layers were completed onto the glass slides (Marienfield, Germany). Syringe pump (Harvard Apparatus, USA), syringe (Becton Dickinson, Sigma-Aldrich, USA), and Tygon® tubing (Tygon® Saint-Gobain, USA) were used to supply flow into microfluidic chip.

In the study, microspheres (Cospheric LLC, CA) were utilized and prepared in Pluronic F-127 (Sigma-Aldrich, USA). DMEM High Glucose with L-Glutamine DMEM (Merck, Germany), Trypsin-EDTA 1X in PBS w/o Ca, Mg w/o, Phenol Red (Euroclone, Italy) and petri dishes (Isolab, Germany) were used during the culturing of U937 and MCF-7 cell lines. Gadavist (Gd) (Bayer, Germany) solution were used to levitate them and microscope images were taken by Zeiss Axio Vert A1 inverted fluorescent microscope (ZEISS, Switzerland). Results were analyzed by Graphpad Prism 8 (GraphPad Software, Inc, USA).

5.2.1. Experimental Setup

The microfluidic chip placed between two magnets with opposite poles 1.5 mm apart consists of a 150 μm DSA film layer between the upper and lower glass of 1 mm and 170 μm thickness (Figure 5.1.). Channel dimensions are 8 mm wide x 4.5 cm long x 150 μm height.

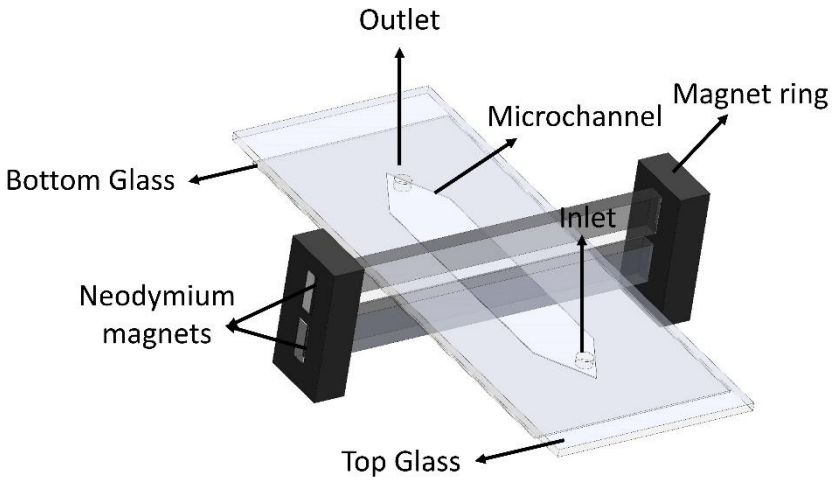

Figure 5.1. Negative magnetophoresis chip composed of two magnets one at the top and the bottom.

Since microparticles are diamagnetic, the particles tend to move low magnetic field regions due to negative magnetophoresis. Therefore, magnetic forces (F_M) on microparticles near the magnets are opposite the microfluidic drag forces (F_D). So, at the adequate flow rate, small particles are flown away while the large particles are captured near the magnets (Equation 5.1).

$$F_M + F_D = \frac{V(\chi_m - \chi_p)}{\mu_o}(B.\nabla)B + 6\pi R\eta f_D v \quad (5.1)$$

V is the volume of the particle, χp and χm are the magnetic susceptibility of the particle and the paramagnetic solution, respectively, μ0 is the magnetic permeability of the air (1.2566×10−6 kg·m A−2·s−2), B is the magnetic induction in three-dimensional space, R is the radius of the particle, ∇ is the del operator, η is the dynamic viscosity, v is the particle velocity, and fD is the drag constant.

5.2.2. Size-based Microparticle Separation

It was examined the separation of microparticles with different sizes (15-25 μm) in order to model the separation of tumor cells circulating in the blood (12-25 μm) (Mendelaar et al. 2021), which are larger than red blood cells (7-8 μm) and white blood cells (8-14 μm) in the microfluidic channel (Kinnunen et al. 2011). In experiments, microparticles were prepared in PBS containing 1% Pluronic F-127 and 200 mM paramagnetic Gd. By applying different flow rates, the capturing percentage at each flow rate was calculated and the flow rate at which small particles were passed, while large particles were captured in the magnet region, was determined. In addition, the distribution of the microparticles used was examined.

5.2.3. Size-based Circulating Tumor Cell Separation

Different sizes of human monocytic macrophage cells U937 and breast cancer cells MCF-7 were separated using the negative magnetophoresis chip. Since U937 cells were suspended, they were cultured every 2-3 days and RPMI was used as the medium. During the experiment, U937 cells were used at a concentration of 3.5 x 10^4 cells/mL. Since MCF-7 cells were adherent, they were removed from the surface with trypsin every

2-3 days, washed with PBS and cultured in fresh DMEM medium. During the experiment, MCF-7 cells were used at a concentration of 3.5 x 10^4 cells/mL. For the filtration of the cells, the flow rate was determined using a 200 mM Gd concentration, in which MCF-7 cells were captured in the magnet region and U937 cells were removed from the magnet region with the flow.

5.2.4. Statistical Analysis

Unless stated, all experiments were performed as triplicates using a negative magnetophoresis microfluidic chip. The data are presented as mean ± standard deviation (SD) from the mean values of triplicates. The data of mean value of triplicates are shown in the graph as mean ± standard deviation (SD). The statistical analyses were conducted by two-way analysis of variance (ANOVA) Tukey's multiple comparisons test using GraphPad Prism (version 8.0).

5.3. Results and Discussion

Here, negative magnetophoresis microfluidic chip was applied for size-based microparticle and CTC separation. Since the magnetic forces applied to microparticles and cells of different sizes are different, magnets act as a filter, allowing small microparticles and cells to pass, and capturing the large cells between and in front of the magnet. Besides, the cell deformation seen in the filter structures was also not observed on the system. As a result, larger microparticles (25 μm) and MCF-7 cells can be separated by capturing them between magnets removing of smaller microparticles (15 μm) and U937 cells.

5.3.1. Size-based Microparticle Separation

It was studied on the separation of microparticles of different sizes (15-25 μm) to model the separation of tumor cells circulating in the blood (12-25 μm), which are larger than red blood cells (7-8 μm) and white blood cells (8-14 μm) in the microfluidic channel. As the flow rate increases, the amount of microparticles collected in front of the magnets decreases (Figure 5.2. a). It was observed that 25 μm microparticles were captured

between magnets (>98.5%) more effectively than 15 µm microparticles at 6.5 µL/min flow. It was seen that the percentage of capture in two particles decreases when the flow was increased further. There was a significant difference in the between magnet region capturing rates of 25 µm microparticles at a flow rate of 6 µL/min and 6.5 µL/min ($p<0.05$). These experiments show that large particles can be selectively trapped between magnets over smaller particles. The diameters of 15 µm and 25 µm microparticles were measured as 18.6 ± 1.4 µm and 27.9 ± 1.5 µm, respectively. Their size distribution was examined, and it was observed that their sizes were homogeneous (Figure 5.2. b).

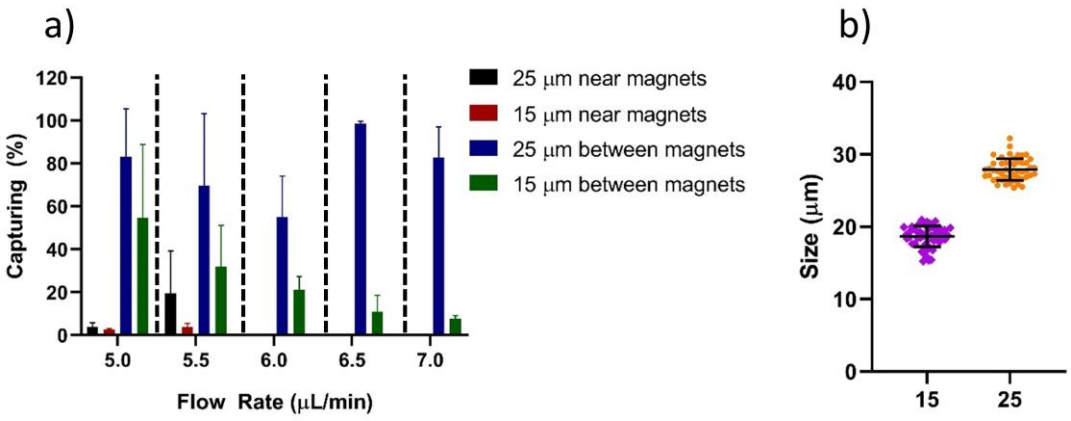

Figure 5.2. Separation of 15 µm and 25 µm microparticles in negative magnetophoresis chip. (a) The capturing (%) of 15 µm and 25 µm microparticles in the magnet region. (b) Size distribution of microparticles.

5.3.2. Size-based Circulating Tumor Cell Separation

It was studied on the separation of U937 and MCF-7 cells. Since the size of the U937 cells is considerably smaller than the MCF-7 cells, it was aimed to find the flow rate where the capturing (%) of U937 cells is low. We were able to reduce the capturing rate from 40.3% at a flow rate of 6 µL/min to 10.94% and 4.53% by increasing the flow rate up to 8 µL/min and 9 µL/min, respectively (Figure 5.3. a). There was no significant difference between the flow rates of the U937 cells in front of the magnet, and a significant difference was obtained for the between magnets at 9 µL/min flow rate compared to 6 µL/min and 7 µL/min flow rates.

Then, we examined the capturing rates of MCF-7 cells at flow rates of 8 µL/min and 9 µL/min, where the capturing rate of U937 cells was low. According to the results, no significant difference was observed between MCF-7 capturing rates at both flow rates, with 90.6% at 8 µL/min and 89.6% at 9 µL/min (Figure 5.3. b) (Figure 5.4.).

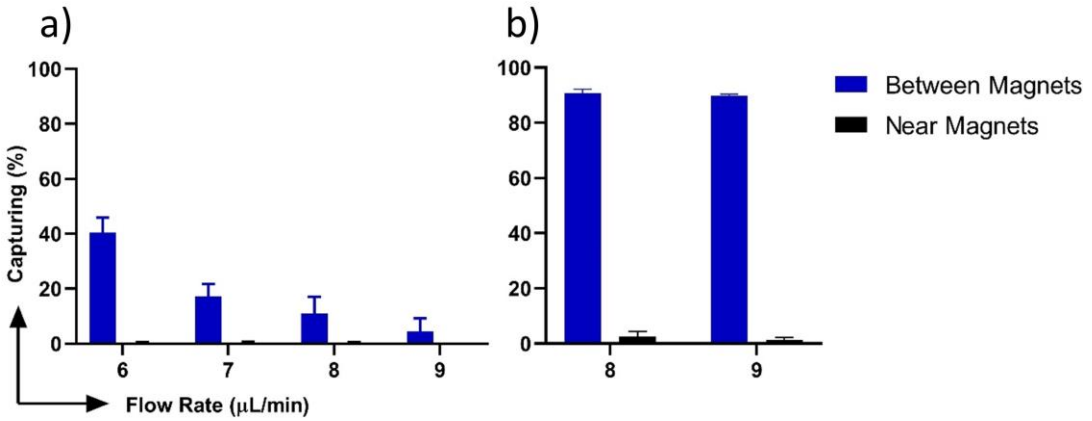

Figure 5.3. Separation of U937 and MCF-7 cells in negative magnetophoresis chip. (a) The capturing (%) of U937 cells with different flow rates. (b) The capturing (%) of MCF-7 cells with different flow rates.

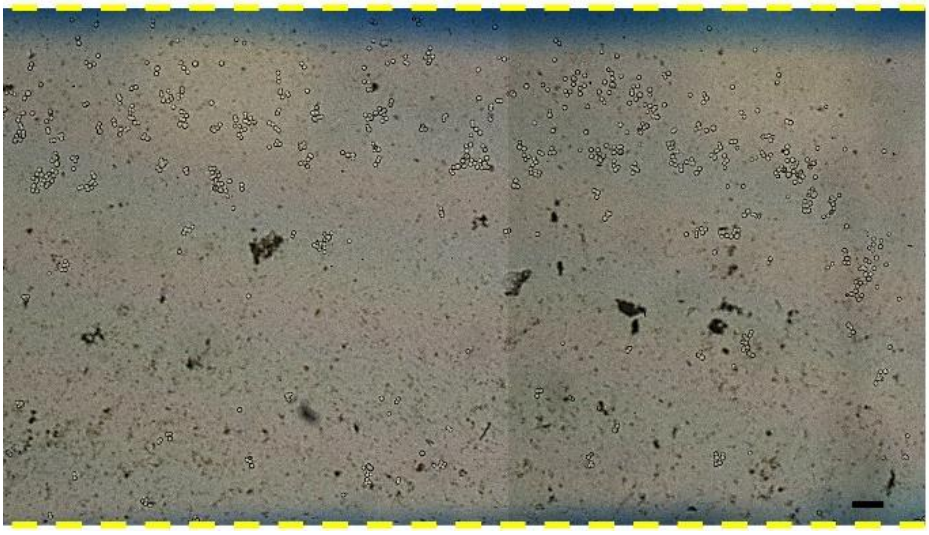

Figure 5.4. Capturing of MCF-7 cells between magnets after removing the magnets.

5.4 Conclusions

In this chapter, we have provided size-dependent microparticle and cell separation within the microfluidic chip with the negative magnetophoresis method. In microfluidics, label-based methods are costly and microstructures, as an example of label-free separation methods, cause low efficiency due to the clogging and deformation. With this study, separation of 15 μm and 25 μm particles using 200 mM Gd for CTC separation modeling was successfully completed. Then, the flow rate at which the smaller size U937 cells will pass through the magnet with 200 mM Gd and the flow rates at which the MCF-7 cells are attached with high efficiency in the magnet region were determined. This study can be further developed for the separation of CTC cells in real patient samples and combined with deep-learning to provide automated analysis by training for different cell types.

CHAPTER 6

CONCLUSION

Cell separation utilizes the features that distinguish cells from each other, thus offers applications such as diagnosis and therapy in many fields. The most important purpose of cell separation studies is to provide separation with as little sample volume and time as possible in a simple and low-cost system with high efficiency and purity. Traditional methods require expensive and bulky devices, complex methods and additional sample processing steps. Centrifugation which is the most basic step of working with cells and clinical samples, is a very difficult approach to implement in microfluidic systems with inlets and outlets. In this context, centrifugal microfluidic systems developed using active and passive elements have pioneered many studies in the field of fluid manipulation and separation. Magnetic-based cell separation studies can separate cells with an easy and label-free method with the effect of magnetic force, which varies according to the size and density difference of the cells.

This thesis has emphasized the advancement of different microfluidic approaches for the cell separation. The thesis consists of two main scopes: i. density-based and size-based microparticle and cell separation ii. Clinical test providing the blood sample separation in a dead-end microfluidics.

For the density-based microparticle separation, a vacuum-integrated closed channel suitable with the centrifuge device was developed and the separation of 1.02-1.09 g/mL microparticles and 1.02-1.05 g/mL microparticles was achieved with 86% for 10 min and 96.3% for 8 minutes at 4000 rpm using the Ficoll density-gradient medium. Besides, it was offered that the filling of a sample in a closed-channel can be provided by the air permeability feature of PDMS. Future work should focus on separation of cells with different densities and collection of separated cells using the syringe from the PDMS chip.

Dead-end channel Spinochip with one reservoir using the centrifugal force was developed, for the first time, for sample manipulations suitable with the centrifuge device. The principle of a system was demonstrated with different channel sizes and various manipulations of a fluid was shown. Moreover, this Spinochip was applied for clinical test of hematocrit measurement and white blood cell estimation from 10 μL of a whole

blood sample in 10 min. It was found that plasma separation from whole blood sample can be obtained with the centrifugal force in the microfluidic channel and it was revealed that, for the first time, a buffy coat region can be observed in a microfluidic chip and WBC estimation made from the thickness of a buffy coat. The results showed that measurements of hematocrit and white blood cells made in Spinochip correlated with the clinical patient results. Further modifications in Spinochip can be made for automatization of fluid manipulations and different clinical tests. Besides, this system can be integrated with the image processing for an automated analysis of results.

A size-based separation of microparticles and circulating tumor cells was also demonstrated in a negative magnetophoresis microfluidic system. It was found that the capturing of 25 μm microparticles from 15 μm microparticles with > 98.5% at 6.5 μL/min flow rate at 200 mM Gd solution. Then, the system was applied capturing of U937 and MCF-7 cells for the CTC separation modeling. With this regard, at 9 μL/min flow rate, 95.47% of U937 cells were removed from the magnets, while a 89.6% of MCF-7 cells were captured between magnets at 200 mM Gd solution. Further, separation of a mixture of cells can be examined in negative magnetophoresis chip and it can be analyzed with real samples. Moreover, this system can be integrated with deep learning to distinguish different cell types.

As conclusion, the results of the studies have shown that novel, cost friendly, sensitive and rapid microfluidic chips advanced in this thesis can contribute the cell separation studies and clinical tests in different fields.

REFERENCES

Aghaamoo, Mohammad, Zhifeng Zhang, Xiaolin Chen, and Jie Xu. 2015. "Deformability-Based Circulating Tumor Cell Separation with Conical-Shaped Microfilters: Concept, Optimization, and Design Criteria." *Biomicrofluidics* 9 (3). AIP Publishing LLC: 034106.

Aghilinejad, Arian, Mohammad Aghaamoo, and Xiaolin Chen. 2019. "On the Transport of Particles/Cells in High-Throughput Deterministic Lateral Displacement Devices: Implications for Circulating Tumor Cell Separation." *Biomicrofluidics* 13 (3). AIP Publishing LLC: 034112.

Al-Faqheri, Wisam, Tzer Hwai Gilbert Thio, Mohammad Ameen Qasaimeh, Andreas Dietzel, Marc Madou, and Ala'aldeen Al-Halhouli. 2017. "Particle/Cell Separation on Microfluidic Platforms Based on Centrifugation Effect: A Review." *Microfluidics and Nanofluidics* 21 (6). Springer: 1–23.

Alieva, Maria, Jacco van Rheenen, and Marike L D Broekman. 2018. "Potential Impact of Invasive Surgical Procedures on Primary Tumor Growth and Metastasis." *Clinical & Experimental Metastasis* 35 (4). Springer: 319–31.

Alvankarian, Jafar, Alireza Bahadorimehr, and Burhanuddin Yeop Majlis. 2013. "A Pillar-Based Microfilter for Isolation of White Blood Cells on Elastomeric Substrate." *Biomicrofluidics* 7 (1). American Institute of Physics: 014102.

Armbruster, David A, David R Overcash, and Jaime Reyes. 2014. "Clinical Chemistry Laboratory Automation in the 21st Century-Amat Victoria Curam (Victory Loves Careful Preparation)." *The Clinical Biochemist Reviews* 35 (3). Australasian Association for Clinical Biochemistry and Laboratory Medicine: 143.

Bacon, Kaitlyn, Ashton Lavoie, Balaji M Rao, Michael Daniele, and Stefano Menegatti. 2020. "Past, Present, and Future of Affinity-Based Cell Separation Technologies." *Acta Biomaterialia* 112. Elsevier: 29–51.

Bankó, Petra, Sun Young Lee, Viola Nagygyörgy, Miklós Zrínyi, Chang Hoon Chae, Dong Hyu Cho, and András Telekes. 2019. “Technologies for Circulating Tumor Cell Separation from Whole Blood.” *Journal of Hematology & Oncology* 12 (1). Springer: 1–20.

Basu, Debdatta, and Rajendra Kulkarni. 2014. “Overview of Blood Components and Their Preparation.” *Indian Journal of Anaesthesia* 58 (5). Wolters Kluwer--Medknow Publications: 529.

Bhagat, Ali Asgar S, Han Wei Hou, Leon D Li, Chwee Teck Lim, and Jongyoon Han. 2011. “Pinched Flow Coupled Shear-Modulated Inertial Microfluidics for High-Throughput Rare Blood Cell Separation.” *Lab on a Chip* 11 (11). Royal Society of Chemistry: 1870–78.

Blumenreich, Martin S. 1990. “The White Blood Cell and Differential Count.” *Clinical Methods: The History, Physical, and Laboratory Examinations. 3rd Edition*. Butterworths.

Buckner, Dean, ROBERT G GRAW JR, Robert J Eisel, Edward S Henderson, and Seymour Perry. 1969. “Leukapheresis* by Continuous Flow Centrifugation (CFC) in Patients with Chronic Myelocytic Leukemia (CML).” *Blood* 33 (2). American Society of Hematology: 353–69.

Bunn, Tang Wai, and Archana Singh Sikarwar. 2016. “Diagnostics: Conventional versus Modern Methods.” *J. Adv. Med. Pharm. Sci* 8: 1–7.

Catarino, Susana O, Raquel O Rodrigues, Diana Pinho, João M Miranda, Graça Minas, and Rui Lima. 2019. “Blood Cells Separation and Sorting Techniques of Passive Microfluidic Devices: From Fabrication to Applications.” *Micromachines* 10 (9). MDPI: 593.

CDC. 2021. “A Quick-Reference Tool for Hemolysis Status.” https://www.cdc.gov/ncezid/dvbd/stories/research-lab-

diagnostics/hemolysispalette.html?CDC_AA_refVal=https%3A%2F%2Fwww.cdc.gov%2Fncezid%2Fdvbd%2Fstories%2Fhemolysis-palette.html.

Chen, Jia-Yang, Wen-Sy Tsai, Hung-Jen Shao, Jen-Chia Wu, Jr-Ming Lai, Si-Hong Lu, Tsung-Fu Hung, Chih-Tsung Yang, Liang-Chun Wu, and Jinn-Shiun Chen. 2016. "Sensitive and Specific Biomimetic Lipid Coated Microfluidics to Isolate Viable Circulating Tumor Cells and Microemboli for Cancer Detection." *PloS One* 11 (3). Public Library of Science San Francisco, CA USA: e0149633.

Chen, Juhong, Chun-Yen Liu, Xinchang Wang, Eric Sweet, Nathaniel Liu, Xiaohua Gong, and Liwei Lin. 2020. "3D Printed Microfluidic Devices for Circulating Tumor Cells (CTCs) Isolation." *Biosensors and Bioelectronics* 150. Elsevier: 111900.

Chen, Peng, Yu-Yen Huang, Gauri Bhave, Kazunori Hoshino, and Xiaojing Zhang. 2016. "Inkjet-Print Micromagnet Array on Glass Slides for Immunomagnetic Enrichment of Circulating Tumor Cells." *Annals of Biomedical Engineering* 44 (5). Springer: 1710–20.

Cheng, Yinuo, Xiongying Ye, Zengshuai Ma, Shuai Xie, and Wenhui Wang. 2016. "High-Throughput and Clogging-Free Microfluidic Filtration Platform for on-Chip Cell Separation from Undiluted Whole Blood." *Biomicrofluidics* 10 (1). AIP Publishing LLC: 014118.

Chin, Elliot K, Colin A Grant, Mehmet Giray Ogut, Bocheng Cai, and Naside Gozde Durmus. 2020. "CelLEVITAS: Label-Free Rapid Sorting and Enrichment of Live Cells via Magnetic Levitation." *BioRxiv*. Cold Spring Harbor Laboratory.

Cho, Hyungseok, Jinho Kim, Hanjung Song, Keun Yong Sohn, MinHyon Jeon, and Ki-Ho Han. 2018. "Microfluidic Technologies for Circulating Tumor Cell Isolation." *Analyst* 143 (13). Royal Society of Chemistry: 2936–70.

Chung, Jaebum, Xiaoze Ou, Rajan P Kulkarni, and Changhuei Yang. 2015. "Counting White Blood Cells from a Blood Smear Using Fourier Ptychographic

Microscopy.” *PloS One* 10 (7). Public Library of Science San Francisco, CA USA: e0133489.

Chung, Jaehoon, Huilin Shao, Thomas Reiner, David Issadore, Ralph Weissleder, and Hakho Lee. 2012. “Microfluidic Cell Sorter (MFCS) for On-chip Capture and Analysis of Single Cells.” *Advanced Healthcare Materials* 1 (4). Wiley Online Library: 432–36.

Civin, Curt I, Tony Ward, Alison M Skelley, Khushroo Gandhi, Zendra Peilun Lee, Christopher R Dosier, Joseph L D’Silva, Yu Chen, MinJung Kim, and James Moynihan. 2016. “Automated Leukocyte Processing by Microfluidic Deterministic Lateral Displacement.” *Cytometry Part A* 89 (12). Wiley Online Library: 1073–83.

Clime, Liviu, Jamal Daoud, Daniel Brassard, Lidija Malic, Matthias Geissler, and Teodor Veres. 2019. “Active Pumping and Control of Flows in Centrifugal Microfluidics.” *Microfluidics and Nanofluidics* 23 (3). Springer: 1–22.

Connes, Philippe, Tamas Alexy, Jon Detterich, Marc Romana, Marie-Dominique Hardy-Dessources, and Samir K Ballas. 2016. “The Role of Blood Rheology in Sickle Cell Disease.” *Blood Reviews* 30 (2). Elsevier: 111–18.

Davari-Tanha, Fatemeh, Mahbod Kaveh, Somayeh Nemati, Pouya Javadian, and Bahram Salmanian. 2014. “Nucleated Red Blood Cells Count in Pregnancies with Idiopathic Intra-Uterine Growth Restriction.” *Journal of Family & Reproductive Health* 8 (2). Tehran University of Medical Sciences: 77.

Delikoyun, Kerem, Sena Yaman, Esra Yilmaz, Oyku Sarigil, Muge Anil-Inevi, Kubra Telli, Ozden Yalcin-Ozuysal, Engin Ozcivici, and H Cumhur Tekin. 2021. “HologLev: A Hybrid Magnetic Levitation Platform Integrated with Lensless Holographic Microscopy for Density-Based Cell Analysis.” *ACS Sensors* 6 (6). ACS Publications: 2191–2201.

Deshmukh, Shreya S, Bikash Shakya, Anna Chen, Naside Gozde Durmus, Bryan Greenhouse, Elizabeth S Egan, and Utkan Demirci. 2021. “Multiparametric Biophysical Profiling of Red Blood Cells in Malaria Infection.” *Communications Biology* 4 (1). Nature Publishing Group: 1–13.

Ding, Xiaoyun, Zhangli Peng, Sz-Chin Steven Lin, Michela Geri, Sixing Li, Peng Li, Yuchao Chen, Ming Dao, Subra Suresh, and Tony Jun Huang. 2014. “Cell Separation Using Tilted-Angle Standing Surface Acoustic Waves.” *Proceedings of the National Academy of Sciences* 111 (36). National Acad Sciences: 12992–97.

Dommett, R M, M T Redaniel, M C G Stevens, W Hamilton, and R M Martin. 2012. “Features of Childhood Cancer in Primary Care: A Population-Based Nested Case–Control Study.” *British Journal of Cancer* 106 (5). Nature Publishing Group: 982–87.

Durmus, Naside Gozde, H Cumhur Tekin, Sinan Guven, Kaushik Sridhar, Ahu Arslan Yildiz, Gizem Calibasi, Ionita Ghiran, Ronald W Davis, Lars M Steinmetz, and Utkan Demirci. 2015. “Magnetic Levitation of Single Cells.” *Proceedings of the National Academy of Sciences* 112 (28). National Acad Sciences: E3661–68.

Farahinia, A, W J Zhang, and I Badea. 2021. “Novel Microfluidic Approaches to Circulating Tumor Cell Separation and Sorting of Blood Cells: A Review.” *Journal of Science: Advanced Materials and Devices*. Elsevier.

Ferreira, Meghaan M, Vishnu C Ramani, and Stefanie S Jeffrey. 2016. “Circulating Tumor Cell Technologies.” *Molecular Oncology* 10 (3). Elsevier: 374–94.

Frenea-Robin, Marie, and Julien Marchalot. 2022. “Basic Principles and Recent Advances in Magnetic Cell Separation.” *Magnetochemistry* 8 (1). MDPI: 11.

Fu, Qibin, Yan Zhang, Tuchen Huang, Ying Liang, and Yang Liu. 2021. “Measurement of Cell Compressibility Changes during Epithelial–Mesenchymal Transition

Based on Acoustofluidic Microdevice." *Biomicrofluidics* 15 (6). AIP Publishing LLC: 064101.

Gascoyne, Peter R C, Sangjo Shim, Jamileh Noshari, Frederick F Becker, and Katherine Stemke-Hale. 2013. "Correlations between the Dielectric Properties and Exterior Morphology of Cells Revealed by Dielectrophoretic Field-flow Fractionation." *Electrophoresis* 34 (7). Wiley Online Library: 1042–50.

Gires, Olivier, and Nikolas H Stoecklein. 2014. "Dynamic EpCAM Expression on Circulating and Disseminating Tumor Cells: Causes and Consequences." *Cellular and Molecular Life Sciences* 71 (22). Springer: 4393–4402.

Gold, B, and M Cankovic. 2015. "Furtado LV, Meier f, Gocke CD: Do Circulating Tumor Cells, Exosomes, and Circulating Tumor Nucleic Acids Have Clinical Utility?: A Report of the Association for Molecular Pathology." *J Mol Diagn* 17: 209–24.

Gossett, Daniel R, Westbrook M Weaver, Albert J Mach, Soojung Claire Hur, Henry Tat Kwong Tse, Wonhee Lee, Hamed Amini, and Dino di Carlo. 2010. "Label-Free Cell Separation and Sorting in Microfluidic Systems." *Analytical and Bioanalytical Chemistry* 397 (8). Springer: 3249–67.

Gronthos, Stan, M Mankani, J Brahim, P Gehron Robey, and Shundi Shi. 2000. "Postnatal Human Dental Pulp Stem Cells (DPSCs) in Vitro and in Vivo." *Proceedings of the National Academy of Sciences* 97 (25). National Acad Sciences: 13625–30.

Habli, Zeina, Walid AlChamaa, Raya Saab, Humam Kadara, and Massoud L Khraiche. 2020. "Circulating Tumor Cell Detection Technologies and Clinical Utility: Challenges and Opportunities." *Cancers* 12 (7). MDPI: 1930.

Haeberle, Stefan, and Roland Zengerle. 2007. "Microfluidic Platforms for Lab-on-a-Chip Applications." *Lab on a Chip* 7 (9). Royal Society of Chemistry: 1094–1110.

Hamacher, Tanja, Johanna T W Berendsen, Jeanne Elisabeth van Dongen, Regine M van der Hee, JJLM Cornelissen, Marleen L W J Broekhuijse, and L I Segerink. 2021. "Virus Removal from Semen with a Pinched Flow Fractionation Microfluidic Chip." *Lab on a Chip* 21 (22). Royal Society of Chemistry: 4477–86.

Hamad, Hussein, and Ankit Mangla. 2019. "Lymphocytosis."

Hao, Si-Jie, Yuan Wan, Yi-Qiu Xia, Xin Zou, and Si-Yang Zheng. 2018. "Size-Based Separation Methods of Circulating Tumor Cells." *Advanced Drug Delivery Reviews* 125. Elsevier: 3–20.

Hassan, U, B Reddy Jr, G Damhorst, O Sonoiki, T Ghonge, C Yang, and R Bashir. 2015. "A Microfluidic Biochip for Complete Blood Cell Counts at the Point-of-Care." *Technology* 3 (04). World Scientific: 201–13.

Hodne, Kjetil, and Finn-Arne Weltzien. 2015. "Single-Cell Isolation and Gene Analysis: Pitfalls and Possibilities." *International Journal of Molecular Sciences* 16 (11). MDPI: 26832–49.

Huang, R, T A Barber, M A Schmidt, R G Tompkins, M Toner, D W Bianchi, R Kapur, and W L Flejter. 2008. "A Microfluidics Approach for the Isolation of Nucleated Red Blood Cells (NRBCs) from the Peripheral Blood of Pregnant Women." *Prenatal Diagnosis: Published in Affiliation with the International Society for Prenatal Diagnosis* 28 (10). Wiley Online Library: 892–99.

Hugo, Suzanne, Kevin Land, Marc Madou, and Horacio Kido. 2014. "A Centrifugal Microfluidic Platform for Point-of-Care Diagnostic Applications." *South African Journal of Science* 110 (1–2). Academy of Science of South Africa: 1–7.

Islam, Muhymin, Hannah Brink, Syndey Blanche, Caleb DiPrete, Tom Bongiorno, Nicholas Stone, Anna Liu, Anisha Philip, Gonghao Wang, and Wilbur Lam. 2017. "Microfluidic Sorting of Cells by Viability Based on Differences in Cell Stiffness." *Scientific Reports* 7 (1). Nature Publishing Group: 1–12.

Jayamohan, Harikrishnan, Himanshu J Sant, and Bruce K Gale. 2013. “Applications of Microfluidics for Molecular Diagnostics.” *Microfluidic Diagnostics*. Springer, 305–34.

Jiang, Youwei, Zhenming Yu, Xinglong Huang, Rifei Chen, Weiyuan Chen, Yifan Zeng, Chengqi Xu, Haodi Min, Nan Zheng, and Xing Cheng. 2018. “A Multilayer Lateral-Flow Microfluidic Device for Particle Separation.” *Microfluidics and Nanofluidics* 22 (4). Springer: 1–7.

Jou, Hei-Jen, Li-Yun Chou, Wen-Chun Chang, Hsin-Cheng Ho, Wan-Ting Zhang, Pei-Ying Ling, Ko-Hsin Tsai, Szu-Hua Chen, Tze-Ho Chen, and Pei-Hsuan Lo. 2021. “An Automatic Platform Based on Nanostructured Microfluidic Chip for Isolating and Identification of Circulating Tumor Cells.” *Micromachines* 12 (5). Multidisciplinary Digital Publishing Institute: 473.

Kasimir-Bauer, Sabine, Oliver Hoffmann, Diethelm Wallwiener, Rainer Kimmig, and Tanja Fehm. 2012. “Expression of Stem Cell and Epithelial-Mesenchymal Transition Markers in Primary Breast Cancer Patients with Circulating Tumor Cells.” *Breast Cancer Research* 14 (1). Springer: 1–9.

Kecili, Seren, and H Cumhur Tekin. 2020. “Adhesive Bonding Strategies to Fabricate High-Strength and Transparent 3D Printed Microfluidic Device.” *Biomicrofluidics* 14 (2). AIP Publishing LLC: 024113.

Kinnunen, Matti, Antti Kauppila, Artashes Karmenyan, and Risto Myllylä. 2011. “Effect of the Size and Shape of a Red Blood Cell on Elastic Light Scattering Properties at the Single-Cell Level.” *Biomedical Optics Express* 2 (7). Optica Publishing Group: 1803–14.

Kong, Matthew C R, Adam P Bouchard, and Eric D Salin. 2012. “Displacement Pumping of Liquids Radially Inward on Centrifugal Microfluidic Platforms in Motion.” *Micromachines* 3 (1). Molecular Diversity Preservation International: 1–9.

Kuan, Da-Han, Chia-Chien Wu, Wei-Yu Su, and Nien-Tsu Huang. 2018. “A Microfluidic Device for Simultaneous Extraction of Plasma, Red Blood Cells, and on-Chip White Blood Cell Trapping.” *Scientific Reports* 8 (1). Nature Publishing Group: 1–9.

Kwon, Seyong, Jieung Oh, Min Seok Lee, Eujin Um, Joonwoo Jeong, and Joo H Kang. 2021. “Enhanced Diamagnetic Repulsion of Blood Cells Enables Versatile Plasma Separation for Biomarker Analysis in Blood.” *Small* 17 (23). Wiley Online Library: 2100797.

LaboratoryInfo. 2022. “Rythrocyte Sedimentation Rate (ESR) : Principle, Methods of Determination and Clinical Significance.” https://laboratoryinfo.com/esr/.

Lamberti, A, S L Marasso, and MJRA Cocuzza. 2014. “PDMS Membranes with Tunable Gas Permeability for Microfluidic Applications.” *Rsc Advances* 4 (106). Royal Society of Chemistry: 61415–19.

Lee, Myung Gwon, Joong Ho Shin, Chae Yun Bae, Sungyoung Choi, and Je-Kyun Park. 2013. “Label-Free Cancer Cell Separation from Human Whole Blood Using Inertial Microfluidics at Low Shear Stress.” *Analytical Chemistry* 85 (13). ACS Publications: 6213–18.

Lenz, Kiersten D, Shailja Jakhar, Jing W Chen, Aaron S Anderson, Dylan C Purcell, Mohammad O Ishak, Jennifer F Harris, Leyla E Akhadov, Jessica Z Kubicek-Sutherland, and Pulak Nath. 2021. “A Centrifugal Microfluidic Cross-Flow Filtration Platform to Separate Serum from Whole Blood for the Detection of Amphiphilic Biomarkers.” *Scientific Reports* 11 (1). Nature Publishing Group: 1–8.

Lin, Danfeng, Lesang Shen, Meng Luo, Kun Zhang, Jinfan Li, Qi Yang, Fangfang Zhu, Dan Zhou, Shu Zheng, and Yiding Chen. 2021. “Circulating Tumor Cells: Biology and Clinical Significance.” *Signal Transduction and Targeted Therapy* 6 (1). Nature Publishing Group: 1–24.

Lin, Shujing, Xiao Zhi, D I Chen, Fangfang Xia, Yihuan Shen, Jiaqi Niu, Shiyi Huang, Jie Song, Jianmin Miao, and Daxiang Cui. 2019. “A Flyover Style Microfluidic Chip for Highly Purified Magnetic Cell Separation.” *Biosensors and Bioelectronics* 129. Elsevier: 175–81.

Lin, Yen-Heng, Shih-Hao Wang, Min-Hsien Wu, Tung-Ming Pan, Chao-Sung Lai, Ji-Dung Luo, and Chiuan-Chian Chiou. 2013. “Integrating Solid-State Sensor and Microfluidic Devices for Glucose, Urea and Creatinine Detection Based on Enzyme-Carrying Alginate Microbeads.” *Biosensors and Bioelectronics* 43. Elsevier: 328–35.

Liu, Zongbin, Rui Chen, Ying Li, Jianqiao Liu, Ping Wang, Xuefeng Xia, and Lidong Qin. 2018. “Integrated Microfluidic Chip for Efficient Isolation and Deformability Analysis of Circulating Tumor Cells.” *Advanced Biosystems* 2 (10). Wiley Online Library: 1800200.

Lombodorj, Batzorig, Horas Cendana Tseng, Hwan-You Chang, Yen-Wen Lu, Namnan Tumurpurev, Chun-Wei Lee, Batdemberel Ganbat, Ren-Guei Wu, and Fan-Gang Tseng. 2020. “High-Throughput White Blood Cell (Leukocyte) Enrichment from Whole Blood Using Hydrodynamic and Inertial Forces.” *Micromachines* 11 (3). MDPI: 275.

Lu, Xinyu, and Xiangchun Xuan. 2015. “Continuous Microfluidic Particle Separation via Elasto-Inertial Pinched Flow Fractionation.” *Analytical Chemistry* 87 (12). ACS Publications: 6389–96.

MacCallum, Iain, Alex Cunningham, and David McKee. 2004. “The Measurement and Modelling of Light Scattering by Phytoplankton Cells at Narrow Forward Angles.” *Journal of Optics A: Pure and Applied Optics* 6 (7). IOP Publishing: 698.

Marjanovič, Igor, Maša Kandušer, Damijan Miklavčič, Mateja Manček Keber, and Mojca Pavlin. 2014. “Comparison of Flow Cytometry, Fluorescence Microscopy

and Spectrofluorometry for Analysis of Gene Electrotransfer Efficiency." *The Journal of Membrane Biology* 247 (12). Springer: 1259–67.

McKinnon, Katherine M. 2018. "Flow Cytometry: An Overview." *Current Protocols in Immunology* 120 (1). Wiley Online Library: 1–5.

Mendelaar, Pauline A J, Jaco Kraan, Mai Van, Leonie L Zeune, Leon W M M Terstappen, Esther Oomen-de Hoop, John W M Martens, and Stefan Sleijfer. 2021. "Defining the Dimensions of Circulating Tumor Cells in a Large Series of Breast, Prostate, Colon, and Bladder Cancer Patients." *Molecular Oncology* 15 (1). Wiley Online Library: 116–25.

Mondal, Himel, and Deepa P Budh. 2019. "Hematocrit."

Moon, Byeong-Ui, Liviu Clime, Daniel Brassard, Alex Boutin, Jamal Daoud, Keith Morton, and Teodor Veres. 2021. "An Automated Centrifugal Microfluidic Assay for Whole Blood Fractionation and Isolation of Multiple Cell Populations Using an Aqueous Two-Phase System." *Lab on a Chip* 21 (21). Royal Society of Chemistry: 4060–70.

Nader, Elie, Marc Romana, and Philippe Connes. 2020. "The Red Blood Cell—Inflammation Vicious Circle in Sickle Cell Disease." *Frontiers in Immunology* 11. Frontiers Media SA: 454.

Nasiri, Rohollah, Amir Shamloo, Samad Ahadian, Leyla Amirifar, Javad Akbari, Marcus J. Goudie, Kang Ju Lee, et al. 2020. "Microfluidic-Based Approaches in Targeted Cell/Particle Separation Based on Physical Properties: Fundamentals and Applications." *Small*.

Nepal, Sabin, Haidong Feng, and Bruce K Gale. 2020. "Optimization of a Microfluidic Spiral Channel Used to Separate Sperm from Blood Cells." *Biomicrofluidics* 14 (6). AIP Publishing LLC: 064103.

Novacco, Marilisa, Valeria Martini, Carmen Grande, and Stefano Comazzi. 2015. "Analytic Errors in Sysmex-generated Hematology Results in Blood from a Dog with Chronic Lymphocytic Leukemia." *Veterinary Clinical Pathology* 44 (3). Wiley Online Library: 337–41.

Okano, Hiromasa, Tomoki Konishi, Toshihiro Suzuki, Takahiro Suzuki, Shinya Ariyasu, Shin Aoki, Ryo Abe, and Masanori Hayase. 2015. "Enrichment of Circulating Tumor Cells in Tumor-Bearing Mouse Blood by a Deterministic Lateral Displacement Microfluidic Device." *Biomedical Microdevices* 17 (3). Springer: 1–11.

Oksuz, Cemre, and H Cumhur Tekin. 2021. "A Vacuum-Integrated Centrifugal Microfluidic Chip for Density-Based Separation of Microparticles." In 2021 IEEE 34th International Conference on Micro Electro Mechanical Systems (MEMS), 1009–11. IEEE.

Osman, Osman, Sylvain Toru, Frédéric Dumas-Bouchiat, N M Dempsey, Naoufel Haddour, L-F Zanini, François Buret, Gilbert Reyne, and Marie Frenea-Robin. 2013. "Microfluidic Immunomagnetic Cell Separation Using Integrated Permanent Micromagnets." *Biomicrofluidics* 7 (5). American Institute of Physics: 054115.

Pinho, Diana, Violeta Carvalho, Inês M Gonçalves, Senhorinha Teixeira, and Rui Lima. 2020. "Visualization and Measurements of Blood Cells Flowing in Microfluidic Systems and Blood Rheology: A Personalized Medicine Perspective." *Journal of Personalized Medicine* 10 (4). MDPI: 249.

Pødenphant, Marie, Neil Ashley, Kamila Koprowska, Kalim U Mir, Maksim Zalkovskij, Brian Bilenberg, Walter Bodmer, Anders Kristensen, and Rodolphe Marie. 2015. "Separation of Cancer Cells from White Blood Cells by Pinched Flow Fractionation." *Lab on a Chip* 15 (24). Royal Society of Chemistry: 4598–4606.

Ribatti, Domenico, Roberto Tamma, and Tiziana Annese. 2020. “Epithelial-Mesenchymal Transition in Cancer: A Historical Overview.” *Translational Oncology* 13 (6). Elsevier: 100773.

Rostami, Peyman, Navid Kashaninejad, Khashayar Moshksayan, Mohammad Said Saidi, Bahar Firoozabadi, and Nam-Trung Nguyen. 2019. “Novel Approaches in Cancer Management with Circulating Tumor Cell Clusters.” *Journal of Science: Advanced Materials and Devices* 4 (1). Elsevier: 1–18.

Sant, Himanshu J, and Bruce K Gale. 2007. “Microscale Field-Flow Fractionation: Theory and Practice.” In *Microfluidic Technologies for Miniaturized Analysis Systems*, 471–521. Springer.

Shen, Yigang, Yaxiaer Yalikun, and Yo Tanaka. 2019. “Recent Advances in Microfluidic Cell Sorting Systems.” *Sensors and Actuators B: Chemical* 282. Elsevier: 268–81.

Sheng, Weian, Tao Chen, Rahul Kamath, Xiangling Xiong, Weihong Tan, and Z Hugh Fan. 2012. “Aptamer-Enabled Efficient Isolation of Cancer Cells from Whole Blood Using a Microfluidic Device.” *Analytical Chemistry* 84 (9). ACS Publications: 4199–4206.

Shields IV, C Wyatt, Catherine D Reyes, and Gabriel P López. 2015. “Microfluidic Cell Sorting: A Review of the Advances in the Separation of Cells from Debulking to Rare Cell Isolation.” *Lab on a Chip* 15 (5). Royal Society of Chemistry: 1230–49.

Song, Hongjun, Jenna M Rosano, Yi Wang, Charles J Garson, Balabhaskar Prabhakarpandian, Kapil Pant, George J Klarmann, Alan Perantoni, Luis M Alvarez, and Eva Lai. 2015. “Continuous-Flow Sorting of Stem Cells and Differentiation Products Based on Dielectrophoresis.” *Lab on a Chip* 15 (5). Royal Society of Chemistry: 1320–28.

StemCell. 2022. “Cell Separation- Buffy Coat.” Accessed May 15. https://www.stemcell.com/media/images/research-area/cell-separation/buffy-coat.jpg.

StemCell Technologies. 2022. “Magnetic Cell Separation and Cell Isolation.” Accessed May 10. https://www.stemcell.com/cell-separation/magnetic-cell-isolation.

Strelkauskas, A J, M Teodorescu, and S Dray. 1975. “Enumeration and Isolation of Human T and B Lymphocytes by Rosette Formation with Antibody-Coated Erythrocytes.” *Clinical and Experimental Immunology* 22 (1). Oxford University Press: 62.

Sun, Jiashu, Yandong Gao, Richard J Isaacs, Kimberly C Boelte, P Charles Lin, Erik M Boczko, and Deyu Li. 2012. “Simultaneous On-Chip DC Dielectrophoretic Cell Separation and Quantitative Separation Performance Characterization.” *Analytical Chemistry* 84 (4). ACS Publications: 2017–24.

Sun, Jiashu, Chao Liu, Mengmeng Li, Jidong Wang, Yunlei Xianyu, Guoqing Hu, and Xingyu Jiang. 2013. “Size-Based Hydrodynamic Rare Tumor Cell Separation in Curved Microfluidic Channels.” *Biomicrofluidics* 7 (1). American Institute of Physics: 011802.

Sun, Yuxi, and Palaniappan Sethu. 2018. “Low-Stress Microfluidic Density-Gradient Centrifugation for Blood Cell Sorting.” *Biomedical Microdevices* 20: 77su.

Tang, Man, Cong-Ying Wen, Ling-Ling Wu, Shao-Li Hong, Jiao Hu, Chun-Miao Xu, Dai-Wen Pang, and Zhi-Ling Zhang. 2016. “A Chip Assisted Immunomagnetic Separation System for the Efficient Capture and in Situ Identification of Circulating Tumor Cells.” *Lab on a Chip* 16 (7). Royal Society of Chemistry: 1214–23.

Tasoglu, Savas, Joseph A Khoory, Huseyin C Tekin, Clemence Thomas, Antoine E Karnoub, Ionita C Ghiran, and Utkan Demirci. 2015. “Levitational Image

Cytometry with Temporal Resolution." *Advanced Materials* 27 (26). Wiley Online Library: 3901–8.

Thachil, Jecko, and Imelda Bates. 2017. "Approach to the Diagnosis and Classification of Blood Cell Disorders." *Dacie and Lewis Practical Haematology*. Elsevier, 497.

Tian, Fei, Lili Cai, Jianqiao Chang, Shanshan Li, Chao Liu, Tiejun Li, and Jiashu Sun. 2018. "Label-Free Isolation of Rare Tumor Cells from Untreated Whole Blood by Interfacial Viscoelastic Microfluidics." *Lab on a Chip* 18 (22). Royal Society of Chemistry: 3436–45.

Tomaiuolo, Giovanna. 2014. "Biomechanical Properties of Red Blood Cells in Health and Disease towards Microfluidics." *Biomicrofluidics* 8 (5). AIP Publishing LLC: 051501.

Tomlinson, Matthew J, Sophie Tomlinson, Xuebin B Yang, and Jennifer Kirkham. 2013. "Cell Separation: Terminology and Practical Considerations." *Journal of Tissue Engineering* 4. SAGE Publications Sage UK: London, England: 2041731412472690.

Toss, Angela, Zhaomei Mu, Sandra Fernandez, and Massimo Cristofanilli. 2014. "CTC Enumeration and Characterization: Moving toward Personalized Medicine." *Annals of Translational Medicine* 2 (11). AME Publications.

Tottori, Naotomo, Takasi Nisisako, Jongho Park, Yasuko Yanagida, and Takeshi Hatsuzawa. 2016. "Separation of Viable and Nonviable Mammalian Cells Using a Deterministic Lateral Displacement Microfluidic Device." *Biomicrofluidics* 10 (1). AIP Publishing LLC: 014125.

Trang, Dai Thi Xuan, Nguyen Tien Huy, Tohru Kariu, Kunihiko Tajima, and Kaeko Kamei. 2004. "One-Step Concentration of Malarial Parasite-Infected Red Blood Cells and Removal of Contaminating White Blood Cells." *Malaria Journal* 3 (1). BioMed Central: 1–7.

Tvedten, Harold, and Rose E Raskin. 2012. “Leukocyte Disorders.” *Small Animal Clinical Diagnosis by Laboratory Methods*. Elsevier, 63.

Wada, Seiji, and Michihiro Kitagawa. 2004. “Method of Separation and Concentration of Fetal Nucleated Red Blood Cells in Maternal Blood and Its Application to Fetal Diagnosis.” *Congenital Anomalies* 44 (2). Wiley Online Library: 72–78.

Wang, Ji Yi, Dong Kai Zhen, Vincent M Falco, Antonio Farina, Yuen Ling Zheng, L C Delli-Bovi, and Diana W Bianchi. 2000. “Fetal Nucleated Erythrocyte Recovery: Fluorescence Activated Cell Sorting-based Positive Selection Using Anti-gamma Globin versus Magnetic Activated Cell Sorting Using Anti-CD45 Depletion and Anti-gamma Globin Positive Selection.” *Cytometry: The Journal of the International Society for Analytical Cytology* 39 (3). Wiley Online Library: 224–30.

Warkiani, Majid Ebrahimi, Lidan Wu, Andy Kah Ping Tay, and Jongyoon Han. 2015. “Large-Volume Microfluidic Cell Sorting for Biomedical Applications.” *Annual Review of Biomedical Engineering* 17. Annual Reviews: 1–34.

Williams, S Kim Ratanathanawongs, J Ray Runyon, and Akram A Ashames. 2011. “Field-Flow Fractionation: Addressing the Nano Challenge.” ACS Publications.

Wu, Ling-Ling, Man Tang, Zhi-Ling Zhang, Chu-Bo Qi, Jiao Hu, Xu-Yan Ma, and Dai-Wen Pang. 2018. “Chip-Assisted Single-Cell Biomarker Profiling of Heterogeneous Circulating Tumor Cells Using Multifunctional Nanospheres.” *Analytical Chemistry* 90 (17). ACS Publications: 10518–26.

Wu, Ling-Ling, Zhi-Ling Zhang, Man Tang, Dong-Liang Zhu, Xiao-Juan Dong, Jiao Hu, Chu-Bo Qi, Hong-Wu Tang, and Dai-Wen Pang. 2020. “Spectrally Combined Encoding for Profiling Heterogeneous Circulating Tumor Cells Using a Multifunctional Nanosphere-Mediated Microfluidic Platform.” *Angewandte Chemie International Edition* 59 (28). Wiley Online Library: 11240–44.

Xiang, Nan, Jie Wang, Qiao Li, Yu Han, Di Huang, and Zhonghua Ni. 2019. “Precise Size-Based Cell Separation via the Coupling of Inertial Microfluidics and Deterministic Lateral Displacement.” *Analytical Chemistry* 91 (15). ACS Publications: 10328–34.

Xu, Yan, Jianhui Xie, Ronghua Chen, Yu Cao, Yuan Ping, Qingwen Xu, Wei Hu, Dan Wu, Lihua Gu, and Huaigu Zhou. 2016. “Fluorescence-and Magnetic-Activated Cell Sorting Strategies to Separate Spermatozoa Involving Plural Contributors from Biological Mixtures for Human Identification.” *Scientific Reports* 6 (1). Nature Publishing Group: 1–12.

Yamada, Masumi, Megumi Nakashima, and Minoru Seki. 2004. “Pinched Flow Fractionation: Continuous Size Separation of Particles Utilizing a Laminar Flow Profile in a Pinched Microchannel.” *Analytical Chemistry* 76 (18). ACS Publications: 5465–71.

Yaman, Sena, Muge Anil-Inevi, Engin Ozcivici, and H Cumhur Tekin. 2018. “Magnetic Force-Based Microfluidic Techniques for Cellular and Tissue Bioengineering.” *Frontiers in Bioengineering and Biotechnology* 6. Frontiers Media SA: 192.

Yang, Z-W, S-H Yang, L Chen, J Qu, J Zhu, and Z Tang. 2001. “Comparison of Blood Counts in Venous, Fingertip and Arterial Blood and Their Measurement Variation.” *Clinical & Laboratory Haematology* 23 (3). Wiley Online Library: 155–59.

Yoon, Yousang, Seonil Kim, Jusin Lee, Jaewoong Choi, Rae-Kwon Kim, Su-Jae Lee, Onejae Sul, and Seung-Beck Lee. 2016. “Clogging-Free Microfluidics for Continuous Size-Based Separation of Microparticles.” *Scientific Reports* 6 (1). Nature Publishing Group: 1–8.

Zeinali, Mina, Vasudha Murlidhar, Shamileh Fouladdel, Shimeng Shao, Lili Zhao, Heather Cameron, Armand Bankhead III, Jiaqi Shi, Kyle C Cuneo, and Vaibhav Sahai. 2018. “Profiling Heterogeneous Circulating Tumor Cells (CTC)

Populations in Pancreatic Cancer Using a Serial Microfluidic CTC Carpet Chip." *Advanced Biosystems* 2 (12). Wiley Online Library: 1800228.

Zeng, Jian, Yanxiang Deng, Pallavi Vedantam, Tzuen-Rong Tzeng, and Xiangchun Xuan. 2013. "Magnetic Separation of Particles and Cells in Ferrofluid Flow through a Straight Microchannel Using Two Offset Magnets." *Journal of Magnetism and Magnetic Materials* 346. Elsevier: 118–23.

Zhang, Fan, Lili Wu, Weidong Nie, Lili Huang, Jinfeng Zhang, Feng Li, and Hai-Yan Xie. 2019. "Biomimetic Microfluidic System for Fast and Specific Detection of Circulating Tumor Cells." *Analytical Chemistry* 91 (24). ACS Publications: 15726–31.

Zhang, Hongyi, Xiaoyan Lin, Yuan Huang, Minghong Wang, Chunmei Cen, Shasha Tang, Marcia R Dique, Lu Cai, Manuel A Luis, and Jillian Smollar. 2021. "Detection Methods and Clinical Applications of Circulating Tumor Cells in Breast Cancer." *Frontiers in Oncology* 11. Frontiers: 1816.

Zhang, Peiran, Hunter Bachman, Adem Ozcelik, and Tony Jun Huang. 2020. "Acoustic Microfluidics." *Annual Review of Analytical Chemistry (Palo Alto, Calif.)* 13 (1). NIH Public Access: 17.

Zhao, Kai, Larasati, Bernard P Duncker, and Dongqing Li. 2019. "Continuous Cell Characterization and Separation by Microfluidic Alternating Current Dielectrophoresis." *Analytical Chemistry* 91 (9). ACS Publications: 6304–14.

Zhu, Yunzeng, Yiqi Chen, and Youchun Xu. 2018. "Interruptible Siphon Valving for Centrifugal Microfluidic Platforms." *Sensors and Actuators B: Chemical* 276. Elsevier: 313–21.

APPENDIX A.

ETHICAL APPROVAL

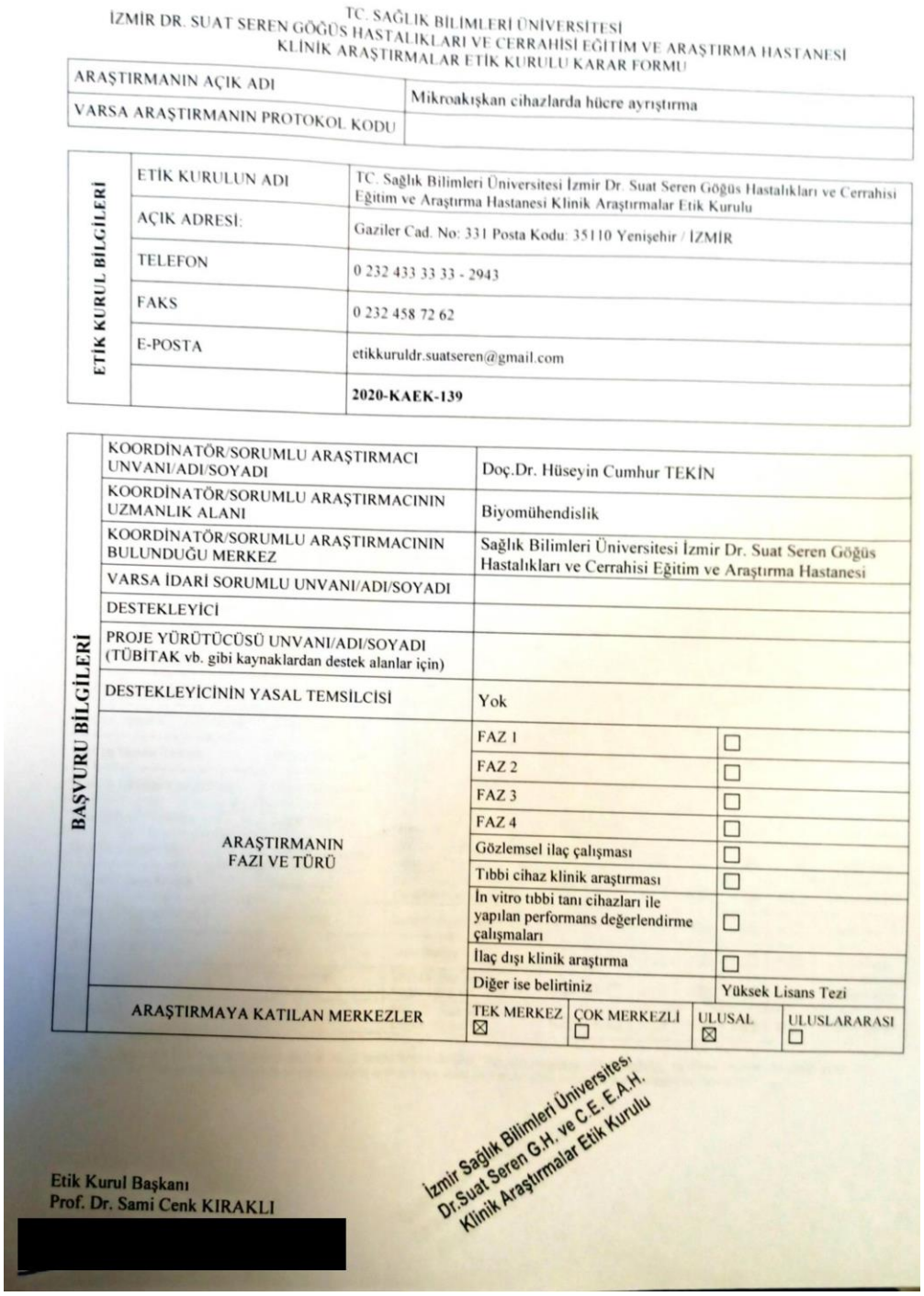

TC. SAĞLIK BİLİMLERİ ÜNİVERSİTESİ
İZMİR DR. SUAT SEREN GÖĞÜS HASTALIKLARI VE CERRAHİSİ EĞİTİM VE ARAŞTIRMA HASTANESİ
KLİNİK ARAŞTIRMALAR ETİK KURULU KARAR FORMU

ARAŞTIRMANIN AÇIK ADI	Mikroakışkan cihazlarda hücre ayrıştırma
VARSA ARAŞTIRMANIN PROTOKOL KODU	

ETİK KURUL BİLGİLERİ		
	ETİK KURULUN ADI	TC. Sağlık Bilimleri Üniversitesi İzmir Dr. Suat Seren Göğüs Hastalıkları ve Cerrahisi Eğitim ve Araştırma Hastanesi Klinik Araştırmalar Etik Kurulu
	AÇIK ADRESİ:	Gaziler Cad. No: 331 Posta Kodu: 35110 Yenişehir / İZMİR
	TELEFON	0 232 433 33 33 - 2943
	FAKS	0 232 458 72 62
	E-POSTA	etikkuruldr.suatseren@gmail.com
		2020-KAEK-139

BAŞVURU BİLGİLERİ					
	KOORDİNATÖR/SORUMLU ARAŞTIRMACI UNVANI/ADI/SOYADI	Doç.Dr. Hüseyin Cumhur TEKİN			
	KOORDİNATÖR/SORUMLU ARAŞTIRMACININ UZMANLIK ALANI	Biyomühendislik			
	KOORDİNATÖR/SORUMLU ARAŞTIRMACININ BULUNDUĞU MERKEZ	Sağlık Bilimleri Üniversitesi İzmir Dr. Suat Seren Göğüs Hastalıkları ve Cerrahisi Eğitim ve Araştırma Hastanesi			
	VARSA İDARİ SORUMLU UNVANI/ADI/SOYADI				
	DESTEKLEYİCİ				
	PROJE YÜRÜTÜCÜSÜ UNVANI/ADI/SOYADI (TÜBİTAK vb. gibi kaynaklardan destek alanlar için)				
	DESTEKLEYİCİNİN YASAL TEMSİLCİSİ	Yok			
	ARAŞTIRMANIN FAZI VE TÜRÜ	FAZ 1	☐		
		FAZ 2	☐		
		FAZ 3	☐		
		FAZ 4	☐		
		Gözlemsel ilaç çalışması	☐		
		Tıbbi cihaz klinik araştırması	☐		
		İn vitro tıbbi tanı cihazları ile yapılan performans değerlendirme çalışmaları	☐		
		İlaç dışı klinik araştırma	☐		
		Diğer ise belirtiniz	Yüksek Lisans Tezi		
	ARAŞTIRMAYA KATILAN MERKEZLER	TEK MERKEZ ☒	ÇOK MERKEZLİ ☐	ULUSAL ☒	ULUSLARARASI ☐

İzmir Sağlık Bilimleri Üniversitesi
Dr.Suat Seren G.H. ve C.E. E.A.H.
Klinik Araştırmalar Etik Kurulu

Etik Kurul Başkanı
Prof. Dr. Sami Cenk KIRAKLI

TC. SAĞLIK BİLİMLERİ ÜNİVERSİTESİ
İZMİR DR. SUAT SEREN GÖĞÜS HASTALIKLARI VE CERRAHİSİ EĞİTİM VE ARAŞTIRMA HASTANESİ
KLİNİK ARAŞTIRMALAR ETİK KURULU KARAR FORMU

ARAŞTIRMANIN AÇIK ADI	Mikroakışkan cihazlarda hücre ayrıştırma
VARSA ARAŞTIRMANIN PROTOKOL KODU	

	Belge Adı	Tarihi	Versiyon Numarası	Dili
DEĞERLENDİRİLEN BELGELER	ARAŞTIRMA PROTOKOLÜ			Türkçe ☐ İngilizce ☐ Diğer ☐
	BİLGİLENDİRİLMİŞ GÖNÜLLÜ OLUR FORMU			Türkçe ☐ İngilizce ☐ Diğer ☐
	OLGU RAPOR FORMU			Türkçe ☐ İngilizce ☐ Diğer ☐
	ARAŞTIRMA BROŞÜRÜ			Türkçe ☐ İngilizce ☐ Diğer ☐

DEĞERLENDİRİLEN DİĞER BELGELER	Belge Adı		Açıklama
	SİGORTA	☐	
	ARAŞTIRMA BÜTÇESİ	☐	
	BİYOLOJİK MATERYEL TRANSFER FORMU	☐	
	İLAN	☐	
	YILLIK BİLDİRİM	☐	
	SONUÇ RAPORU	☐	
	GÜVENLİLİK BİLDİRİMLERİ	☐	
	DİĞER:	☐	

KARAR BİLGİLERİ		
	Karar No: 2022/26-33	**Tarih:11.05.2022**

Yukarıda bilgileri verilen başvuru dosyası ile ilgili belgeler araştırmanın çalışmanın gerekçe, amaç, yaklaşım ve yöntemleri dikkate alınarak incelenmiş ve uygun bulunmuş olup araştırmanın çalışmanın başvuru dosyasında belirtilen merkezlerde gerçekleştirilmesinde etik ve bilimsel sakınca bulunmadığına toplantıya katılan etik kurul üye tam sayısının salt çoğunluğu ile karar verilmiştir. İlaç ve Biyolojik Ürünlerin Klinik Araştırmaları Hakkında Yönetmelik kapsamında yer alan araştırmalar çalışmalar için Türkiye İlaç ve Tıbbi Cihaz Kurumu'ndan izin alınması gerekmektedir.

KLİNİK ARAŞTIRMALAR ETİK KURULU	
ETİK KURULUN ÇALIŞMA ESASI	Klinik Araştırmaları Hakkında Yönetmelik, İyi Klinik Uygulamaları Kılavuzu
BAŞKANIN UNVANI / ADI / SOYADI:	Prof. Dr. Sami Cenk KIRAKLI

Unvanı/Adı/Soyadı	Uzmanlık Alanı	Kurumu	Cinsiyet		Araştırma İle ilişki		Katılım*		İmza
Prof. Dr. Sami Cenk KIRAKLI	Göğüs Hastalıkları	SBÜ Dr. Suat Seren Göğüs HC EAH	E ☒	K ☐	E ☐	H ☒	E ☒	H ☐	Online katıldı
Prof. Dr. Kenan Can CEYLAN	Göğüs Cerrahi	SBÜ Dr. Suat Seren Göğüs HC EAH	E ☐	K ☒	E ☐	H ☒	E ☒	H ☐	Online katıldı
Prof. Dr. Semra BİLAÇEROĞLU	Göğüs Hastalıkları	SBÜ Dr. Suat Seren Göğüs HC EAH	E ☒	K ☐	E ☐	H ☒	E ☒	H ☐	Online katıldı
Prof. Dr. Dursun TATAR	Göğüs Hastalıkları	SBÜ Dr. Suat Seren Göğüs HC EAH	E ☐	K ☒	E ☐	H ☒	E ☒	H ☐	Online katıldı
Doç. Dr. Gülistan KARADENİZ	Göğüs Hastalıkları	SBÜ Dr. Suat Seren Göğüs HC EAH	E ☐	K ☒	E ☐	H ☒	E ☒	H ☐	Online katıldı
Doç. Dr.Yelda VAROL	Göğüs Hastalıkları	SBÜ Dr. Suat Seren Göğüs HC EAH	E ☐	K ☒	E ☐	H ☒	E ☒	H ☐	Online katıldı
Doç. Dr. Can BİÇMEN	Tıbbi Mikrobiyoloji	SBÜ Dr. Suat Seren Göğüs HC EAH	E ☒	K ☐	E ☒	H ☐	E ☒	H ☐	Online katıldı
Doç. Dr. Gönen SÖZER	Farmakoloji	Ege Üniversitesi Eczacılık Fakültesi Farmakoloji AD.	E ☐	K ☒	E ☐	H ☒	E ☒	H ☐	Online katıldı
Uzman Dr. Gökben YASLI	Halk Sağlığı	İzmir İl Sağlık Müdürlüğü	E ☐	K ☒	E ☐	H ☒	E ☒	H ☐	Online katıldı
Avukat Nuray TÜLEK	Hukuk	İzmir Barosu	E ☐	K ☒	E ☐	H ☒	E ☐	H ☒	Katılmadı
Onur OKUR	Biyomedikal Mühendis	SBÜ Dr. Suat Seren Göğüs HC EAH	E ☒	K ☐	E ☐	H ☒	E ☒	H ☐	Online katıldı
İbrahim KÜÇÜKSÜSLÜ	Sivil Üye	SBÜ Dr. Suat Seren Göğüs HC EAH	E ☒	K ☐	E ☐	H ☒	E ☒	H ☐	Online katıldı

***:Toplantıda Bulunma**
(Klinik Araştırmalar Etik Kurulu toplantısı **online** olarak gerçekleştirilmiş olup "**üye tam sayısının salt çoğunluğu**" ile alınan kararlar elektronik ya da ıslak imzalı karar formları ile etik kurul başkanına iletilmelerinin ardından etik kurul başkanının ıslak imzasıyla başvuru sahibine iletilmiştir)

İzmir Sağlık Bilimleri Üniversitesi
Dr.Suat Seren G.H. ve C.E. E.A.H.
Klinik Araştırmalar Etik Kurulu

Etik Kurul Başkanı
Prof. Dr. Sami Cenk KIRAKLI